

# Journal of Fluid Mechanics

<http://journals.cambridge.org/FLM>

Additional services for **Journal of Fluid Mechanics**:

Email alerts: [Click here](#)

Subscriptions: [Click here](#)

Commercial reprints: [Click here](#)

Terms of use : [Click here](#)



---

## On the refraction of shock waves at a slow–fast gas interface

L. F. Henderson, P. Colella and E. G. Puckett

Journal of Fluid Mechanics / Volume 224 / March 1991, pp 1 - 27

DOI: 10.1017/S0022112091001623, Published online: 26 April 2006

**Link to this article:** [http://journals.cambridge.org/abstract\\_S0022112091001623](http://journals.cambridge.org/abstract_S0022112091001623)

**How to cite this article:**

L. F. Henderson, P. Colella and E. G. Puckett (1991). On the refraction of shock waves at a slow–fast gas interface. *Journal of Fluid Mechanics*, 224, pp 1-27 doi:10.1017/S0022112091001623

**Request Permissions :** [Click here](#)

# On the refraction of shock waves at a slow–fast gas interface

By L. F. HENDERSON†, P. COLELLA‡ AND E. G. PUCKETT¶

Lawrence Livermore National Laboratory, Livermore, CA 94550, USA

(Received 24 November 1989 and in revised form 12 June 1990)

We present the results of numerical computations of the refraction of a plane shock wave at a  $\text{CO}_2/\text{CH}_4$  gas interface. The numerical method was an operator split version of a second-order Godunov method, with adaptive grid refinement. We solved the unsteady, two-dimensional, compressible, Euler equations numerically, assuming perfect gas equations of state, and compared our results with the experiments of Abd-El-Fattah & Henderson. Good agreement was usually obtained, especially when the contamination of the  $\text{CH}_4$  by the  $\text{CO}_2$  was taken into account. Remaining discrepancies were ascribed to the uncertainties in measuring certain wave angles, due to sharp curvature, poor definition, or short length of the waves at large angles of incidence. All the main features of the regular and irregular refractions were resolved numerically for shock strengths that were weak, intermediate, or strong. These include free precursor shock waves in the intermediate and strong cases, evanescent (smeared out) compressions in the weak case, and the appearance of an extra expansion wave in the bound precursor refraction (BPR). The structure of a BPR was elucidated for the first time.

## 1. Introduction

We consider two gases meeting along a plane interface, and we assume for simplicity that they both obey the perfect gas equation of state (figure 1). We suppose that a plane incident shock  $i$  of wave velocity  $U_i$  is propagated into one of the gases by the impulsive motion of a rigid boundary, such as a piston which drives into the gas at a velocity  $U_{pi}$  with  $|U_{pi}| < |U_i|$ . We also assume that all the boundaries of the system are adiabatic. Subsequently  $i$  meets the interface between the gases at an angle of incidence  $\alpha_i = 0$  measured with respect to the interface. The shock  $i$  now begins to pass from the first, or incident gas I, into the second, or receiving gas II, where it becomes the transmitted shock  $t$ . When its new velocity  $U_t$  differs in magnitude from  $U_i$ , then by definition  $i$  has been refracted. Formally the relative refractive index  $n$  is defined by (Henderson 1989)

$$n \equiv \frac{|U_i|}{|U_t|}. \quad (1.1)$$

† Permanent address: The Institute of Space and Astronautical Science, 3-1-1 Yoshinodai, Sagamihara, Kanagawa, 229, Japan.

‡ Permanent address: Department of Mechanical Engineering, University of California, Berkeley, CA 94720, USA.

¶ Permanent address: Department of Mathematics, University of California, Davis, CA 95615, USA.

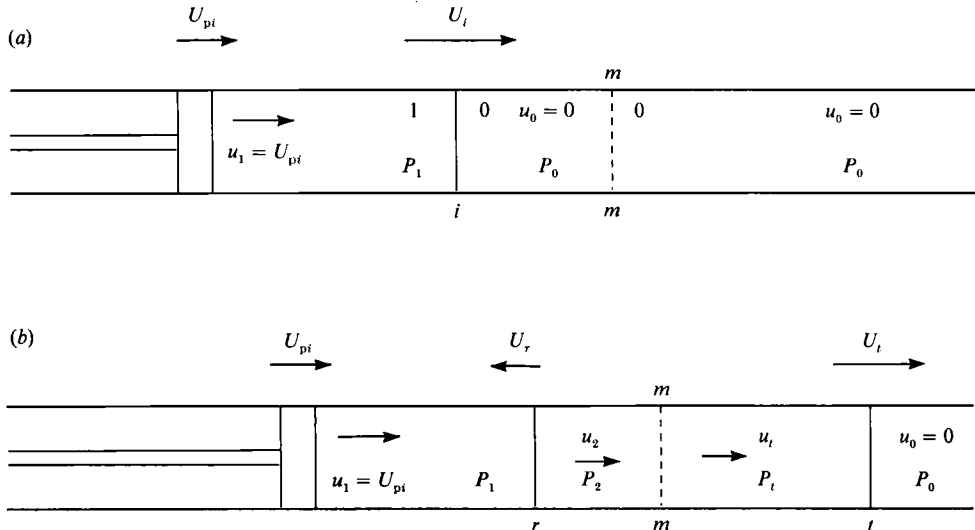


FIGURE 1. Refraction of a normal shock wave  $i$  at zero angle of incidence,  $\alpha_i = 0$ , at a plain interface between two media: (a) before refraction; (b) after refraction.

The refraction is slow-fast when  $n < 1$ ; fast-slow when  $n > 1$ ; and there is no refraction when  $n = 1$ .

If in laboratory frame the velocities of the gas upstream and downstream of the incident shock are  $u_0$  and  $u_1$  respectively, then the piston velocity is

$$U_{pi} = u_i - u_0.$$

In this frame of reference the gas upstream of  $i$  is undisturbed, so that  $u_0 = 0$ , and the boundary condition then becomes simply,  $U_{pi} = u_1$ .

In general a reflected wave is also produced at the gas interface by the refraction (figure 1b). When  $i$  is a shock then so also will be  $t$ , but the reflected wave may be either an expansion  $e$ , or a shock  $r$ . It is assumed that there is always continuity in the pressure  $P$  and in the particle velocity  $u$  across the interface. Following refraction this gives

$$P_2 = P_t, \quad (1.2)$$

$$u_2 = u_t. \quad (1.3)$$

The nature of the reflected wave may be determined with the help of (1.2) and (1.3) together with the notion of wave impedance  $Z$ . For head-on refraction at angle of incidence  $\alpha_i = 0$  the incident wave impedance,  $Z_i$ , is defined by

$$Z_i \equiv \frac{P_1 - P_0}{u_1 - u_0} = \frac{P_1 - P_0}{U_{pi}}.$$

Alternatively, in shock wave coordinates we have

$$Z_i = -\frac{u_0}{\nu_0} = -\rho_0 u_0 = \rho_0 U_i, \quad (1.4)$$

$$Z_i = -\frac{u_1}{\nu_1} = -\rho_1 u_1, \quad (1.5)$$

where  $\rho$  is the density,  $\nu$  is the specific volume, and we have used the fact that in shock wave coordinates  $u_0 = -U_i$ . (In general, an upper case  $U$  ( $U_i$ ,  $U_{pt}$ , etc.) always denotes a velocity with respect to laboratory coordinates whereas a small case  $u$  ( $u_0$ ,  $u_1$ , etc.) may denote a velocity in laboratory coordinates or shock wave coordinates depending on the context.) The transmitted and reflected wave impedances  $Z_t$  and  $Z_r$  are defined similarly. The pressure reflection ( $R$ ) and transmission ( $T$ ) coefficients are

$$R \equiv \frac{P_2 - P_1}{P_1 - P_0} = \frac{Z_r Z_t - Z_i}{Z_i Z_t - Z_r}, \quad (1.6)$$

$$T \equiv \frac{P_t - P_0}{P_1 - P_0} = \frac{Z_t Z_i - Z_r}{Z_i Z_t - Z_r}, \quad (1.7)$$

with similar expressions for the shock intensity which is the average power flux through unit area in the direction of propagation, and the coefficient for the total power transmitted (Henderson 1989). The coefficients (1.6) and (1.7) show that when the impedance increases during refraction  $|Z_t| > |Z_i|$ , then a shock  $r$  will be reflected from the interface back into the incident gas because then  $R > 0$ , but that when it decreases  $|Z_t| < |Z_i|$ , then we obtain a reflected expansion with  $R < 0$ . When the impedances are equal,  $Z_t = Z_i$ , there is no reflected wave even though the two gases may differ in composition or in states. In this case  $R = 0$ . Now combining (1.4) for  $Z_i$  and  $Z_t$  with (1.1) we obtain

$$n = \frac{|U_i|}{|U_t|} = \frac{\nu_0 Z_i}{\nu_t Z_t}, \quad (1.8)$$

where  $\nu_t$  is the specific volume of the gas upstream of the  $t$  shock. So even with  $Z_t = Z_i$ , the wave will still be refracted if  $\nu_t \neq \nu_0$ .

More generally, the incident shock may meet the gas interface at a non-zero angle of incidence  $\alpha_i \neq 0$  (figure 2a), and different refraction phenomena then occur. The wave systems illustrated in figure 2(a–c) are called *regular refractions* by analogy with von Neumann's (1943) classification of regular and Mach *reflections*. His theory of regular reflection is easily extended to regular refraction and the results are in good agreement with experiment (Jahn 1956; Abd-El-Fattah, Henderson & Lozzi 1976; Abd-El-Fattah & Henderson 1978a, b).

If a regular wave system is to exist, then all of its waves must travel at the same velocity  $U$  along the interface, and this fact gives immediately the *fundamental law of refraction*, namely

$$|U| = \frac{|U_i|}{\sin \alpha_i} = \frac{|U_t|}{\sin \alpha_t} = \frac{|U_r|}{\sin \alpha_r} = \frac{|U_j|}{\sin \alpha_j}, \quad (1.9)$$

where  $U_j$  is the velocity of any wave in the reflected and centred expansion wave, and  $\alpha_j$  is the corresponding wave angle (figure 2c). Evidently,  $|U_j| = c_j$ , which is the local speed of sound. Under certain conditions this law may be violated; for example with a continuous increase in the parameter  $\alpha_i$  the regular wave system may break up with the  $t$  shock moving ahead of the incident and reflected waves to form some type of irregular refraction with precursor waves (figure 2d–f). In this event,

$$\frac{|U_t|}{\sin \alpha_t} > \frac{|U_i|}{\sin \alpha_i} = \frac{|U_r|}{\sin \alpha_r} = \frac{|U_j|}{\sin \alpha_j}. \quad (1.10)$$

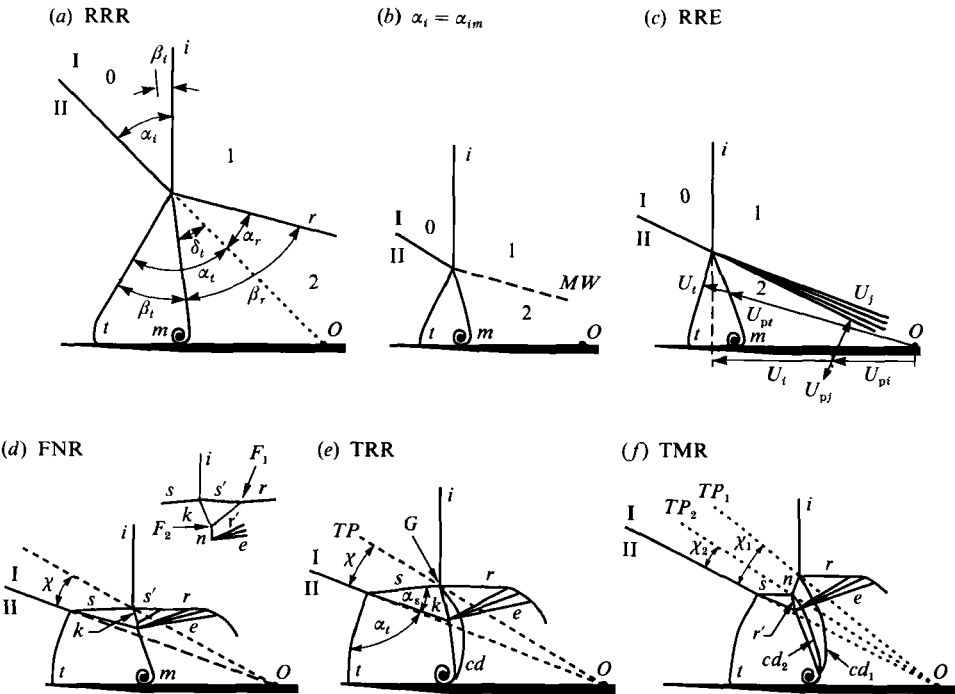


FIGURE 2. (a–c) Regular and (d–f) irregular shock refraction systems for a slow–fast  $\text{CO}_2/\text{CH}_4$  gas interface,  $n < 1$ . (a) Reflected shock, RRR,  $|Z_i| > |Z_t|$ ,  $\alpha_i > \alpha_t$ ; (b) reflected Mach line degeneracy,  $|Z_i| = |Z_t|$ ,  $\alpha_i > \alpha_t = \alpha_{im}$ ; (c) reflected expansion, RRE,  $|Z_i| < |Z_t|$ ,  $\alpha_t > \alpha_i$ ; (d) free precursor von Neumann refraction, FNR; (e) twin regular reflection-refraction, TRR; (f) twin Mach reflection-refraction, TMR.  $i$ , Incident shock;  $t$ , transmitted shock;  $r, r'$ , reflected shocks;  $e$ , reflected expansion wave;  $k$ , modified incident shock;  $n$  Mach shock;  $s$ , side shock;  $s'$ , modified side shock,  $m$  gas interface; I, Region of undisturbed  $\text{CO}_2$ ; II, region of undisturbed  $\text{CH}_4$ ; MW, Mach line;  $cd_{(1,2)}$ , contact discontinuity;  $TP_{(1,2)}$ , trajectory path of shock wave confluences;  $\chi_{(1,2)}$ , trajectory path angles of shock wave confluences;  $F_{1,2}$ , shock triple points;  $G$ , quadruple point;  $O$  origin where  $i$  first encountered gas interface.

For oblique refraction,  $\alpha_i > 0$ , it is necessary to generalize the definition of wave impedance to

$$Z_i \equiv \frac{P_i - P_0}{U_{pi} \cos \beta_i},$$

where  $\beta_i$  is the wave angle measured with respect to the *disturbed* gas interface (figure 2a). Similar expressions are defined for the other waves, and with these definitions (1.6) and (1.7) remain valid.

The refraction law (1.9) may be combined with the definitions of  $n$ ,  $Z_i$ , and  $Z_t$  to extend (1.8) to

$$n = \frac{|U_i|}{|U_t|} = \frac{\sin \alpha_i}{\sin \alpha_t} = \frac{\nu_0 Z_i \cos \beta_i}{\nu_t Z_t \cos \beta_t}. \quad (1.11)$$

The particular angle  $\alpha_i$  for which there is equality of impedance,  $Z_i = Z_t$ , is called the *angle of intromission*  $\alpha_i = \alpha_{im}$ , as in acoustic theory. The wave  $i$  is still refracted at this condition because in general  $n \neq 1$  when  $\alpha_i = \alpha_{im}$  (figure 2b).

Using the refraction law we may also write

$$\cos \alpha_t = (1 - \sin^2 \alpha_t)^{\frac{1}{2}} = (1 - n^{-2} \sin^2 \alpha_i)^{\frac{1}{2}}.$$

Thus  $\cos \alpha_i$  becomes pure imaginary when  $1 - n^{-2} \sin^2 \alpha_i < 0$ , that is when  $\alpha_i$  exceeds the *normal critical angle*,  $\alpha_c$ , which is defined by

$$\sin \alpha_c = n = \frac{|U_i|}{|U_t|}. \quad (1.12)$$

Clearly  $\alpha_c$  only exists for slow–fast refraction,  $n < 1$ . At the critical condition,  $t$  is perpendicular to the gas interface  $\alpha_t = \frac{1}{2}\pi$ ; that is, it is a normal shock. Accordingly the gas interface is not deflected in this special case and it remains everywhere in a single plane. It follows that when the pressure  $P_2$  is applied to the receiving gas it causes no deflection of the interface, so that it behaves like a rigid surface. In this sense  $|Z_t| = \infty$ , when  $\alpha_i = \alpha_c$ . In summary, by (1.11)  $n$  is a measure of the capacity of the gases to bend or refract the incident shock, while by (1.6) and (1.7) the wave impedances determine the nature of the reflected and transmitted waves.

Whitham's (1958, 1959) theory has been extended in an attempt to describe both regular and irregular refractions (Catherasoo & Sturtevant 1983; Schwendeman 1988). It is attractive not only for its simplicity but also because it often agrees remarkably well with experiment. However, it is an approximate theory, and it does not describe wave reflections properly, nor disturbances that arise in the downstream flow and subsequently overtake a shock. In refracting systems difficulties can also arise which are apparently associated with the formation of a 'shock–shock' on an interface, or even when one is close to it. Furthermore it cannot deal with shock discontinuities at a gas interface (Catherasoo & Sturtevant 1983).

By contrast the von Neumann theory is exact (within its assumptions) but it is only adequate for describing regions of uniform flow, which restricts it to regular refractions. Irregular refractions have non-uniformities and it is then necessary to solve the equations of motion everywhere in order to obtain an adequate description of the phenomena.

In the present paper, we present the results of our numerical studies of slow–fast refraction with particular emphasis on the irregular systems. The numerical method that we used is an adaption of second-order, finite-difference solution of the Euler and continuity equations for the two-dimensional, unsteady, compressible flow of perfect gases. It is an operator split version of the second-order Godunov method developed by van Leer (1979), Collela & Glaz (1985), and Colella & Woodward (1984). The results are compared with the experimental data of Abd-El-Fattah & Henderson (1978b). Agreement with experiment is satisfactory for much of the data, particularly if allowance is made for the effects of gas contamination in the experiment. Some discrepancies do exist, especially for the  $\alpha_i$  data for irregular systems. This is ascribed to uncertainties in the measurements caused by the sharp curvature of the transmitted wave at large angles of incident  $\alpha_i$ .

## 2. The experiments

The experimental method has been described by Bitondo (1950), Jahn (1956), Abd-El-Fattah *et al.* (1976), and Abd-El-Fattah & Henderson (1978a, b). The experiments of the last named authors appear to be the most extensive and we describe them briefly. A delicate polymer membrane was set up in a shock tube; its functions were to define the initial gas interface as a plane surface, and to prevent the gases from mixing until the incident shock arrived. The mass of the membrane was between 0.5 and  $1.0 \times 10^{-4}$  kg m<sup>-2</sup>, and its thickness was between  $5.5$  and  $6.5 \times 10^{-8}$  m.

In order to set up a slow–fast interface such as CO<sub>2</sub>/CH<sub>4</sub>, the CO<sub>2</sub> was slowly introduced onto one side of the membrane while the CH<sub>4</sub> was introduced onto the other. The gases were continuously circulated through the shock tube to minimize mutual contamination by diffusion and leakage across the membrane. The contamination was monitored continuously by a thermal conductivity meter, and typically the CH<sub>4</sub> was contaminated by about 10% by volume with CO<sub>2</sub>, but the CO<sub>2</sub> was much purer. It should be noted that the volume of CO<sub>2</sub> in the shock tube was about 250 times larger than the CH<sub>4</sub>.

A shock of prescribed inverse strength  $\xi_i \equiv P_0/P_1$ , was started in the CO<sub>2</sub>, and arranged to strike the membrane/gas interface at a predetermined angle of incidence  $\alpha_i$ . The shock shattered the membrane and entered the CH<sub>4</sub>, and was thus refracted. The wave system was photographed by a schlieren optical system, and transducers measured the speed and strength of the incident shock.

Recently, Haas & Sturtevant (1987) have experimented with weak shocks refracting at cylindrical and spherical interfaces. The gases were initially prevented from mixing by the use of plastic membranes or soap bubbles. However, in the interest of simplicity we will confine our attention to plane gas interfaces.

### **3. The computations**

#### *3.1. The numerical method*

We used a second-order finite-difference solution of the Euler and continuity equations on a rectangular grid with reflecting boundary conditions on three sides and inflow boundary conditions on the fourth. The numerical integration of the equations was accomplished with an operator split version of a second-order Godunov method (van Leer 1979; Colella & Woodward 1984). In our implementation we employed the efficient algorithm for the solution of the Riemann problem developed by Colella & Glaz (1985). Since the method is a conservative finite-difference scheme, mass, momentum, and energy were all conserved. The method is accurate to second order in space and time for smooth flow, and captures shocks and other discontinuities with minimum numerical overshoot and dissipation. It has been used quite extensively to compute unsteady shock reflections in gases, and has a demonstrated ability to resolve complex interactions of discontinuities in good agreement with experiment (Glaz *et al.* 1985).

An important feature of the numerical method is that it employs a dynamic regridding strategy called adaptive mesh refinement (AMR). This entails placing a finer, rectangular grid over any region of particular interest or excessive error, with the grid spacing being reduced by an even factor – typically 2 or 4. The boundary of the refined grid always coincided with the cell edges of the coarse grid. Multiple levels of refinement were possible with the maximum number of nested grids being supplied as a parameter by the user. In the present work, we determined those regions that required refinement by estimating the local truncation error in the density, and refining wherever the error was greater than an initially specified amount. In addition, we refined to the maximum extent all multifluid cells (those containing both gases) and all cells lying within two cell widths of a multifluid cell. Special care was taken to ensure that the fluxes on boundaries between coarse and fine grids matched; the details are given by Berger & Colella (1989). Adaptive gridding was a crucial component of our method which enabled us to resolve important features of the flow economically. A typical run with two levels of gridding and a refinement factor of 4 took 10 minutes of CPU time on a CRAY XMP computer.

	Pure carbon dioxide	Pure methane	Contaminated methane
$\gamma$	1.288	1.303	1.301
$\mu$	44.01	16.04	18.84

TABLE 1. Properties of the pure and contaminated gases

The gas interface was modelled using an algorithm of Noh & Woodward (1976) known as SLIC (Simple Line Interface Calculation). Here a number  $f_{ij}$ , between 0 and 1, and called the volume fraction, was associated with each grid cell through which the gas interface passed. This  $f_{ij}$  was the volume fraction of the cell occupied by one of the gases. Obviously the other gas occupied the fraction  $1-f_{ij}$ . During each integration sweep a simple picture of the interface consisting entirely of vertical and horizontal line segments was constructed from this volume fraction information. This was used to determine how much of each gas was convected out of the cell and into adjacent cells on this pass, and hence to update the volume fractions associated with each cell. One of the drawbacks of volume-of-fluid-based interface tracking schemes such as SLIC is that in a region undergoing expansion or compression both of the gases in a multifluid cell will be expanded or compressed equally, in spite of the density differences that may exist between them. To use this method with the present problem we incorporated a scheme due to Colella, Ferguson & Glaz (1990) in which the equations of gas dynamics are supplemented with evolution equations for the volume fraction, total energy, and mass density of each gas in the multifluid cells. This formulation takes into account the compressibility of each gas component in a multifluid cell so as to ensure the correct individual expansions or compressions.

### 3.2. Outline and plan of the numerical work

We shall present the results of our computations as though we had done a series of experiments in a shock tube. This means that in a particular sequence, the ratios of the specific heats  $\gamma_i, \gamma_t$  of the gases and their molecular weights  $\mu_i, \mu_t$  were held constant and so also was  $\xi_i$ . The only parameter that varied through the sequence was  $\alpha_i$ . This was assumed to be initially near the condition for head-on incidence at  $\alpha_i = 0$ ; it was then increased in discrete steps until it approached glancing incidence at  $\alpha_i = \frac{1}{2}\pi$ ; thus  $0 < \alpha_i < \frac{1}{2}\pi$ . A particular refraction was uniquely defined once the values of  $(\gamma_i, \gamma_t, \mu_i, \mu_t, \xi_i, \alpha_i)$  together with the system boundaries were given. Typically the phenomena that appeared from this procedure were a sequence of regular refractions followed by an irregular sequence.

We shall compare our numerical results with the experimental data obtained by Abd-El-Fattah & Henderson (1978b) for the slow–fast,  $n < 1$ ,  $\text{CO}_2/\text{CH}_4$  gas interface. There were two artifacts in those experiments which we took into account in our computations in order to make the comparison as accurate as possible. These were the inertia of the membrane and the contamination of the gases by diffusion and leakage across it.

**Membrane inertia** We calculated the membrane density from the published data, and it was about 680 times denser than  $\text{CO}_2$  at standard conditions. Using this factor in the computations, the membrane was treated as though it were superdense carbon dioxide. Generally its effect was negligible; all we noticed was a slight displacement in the pressure contours when the contours were compared with, and without, the

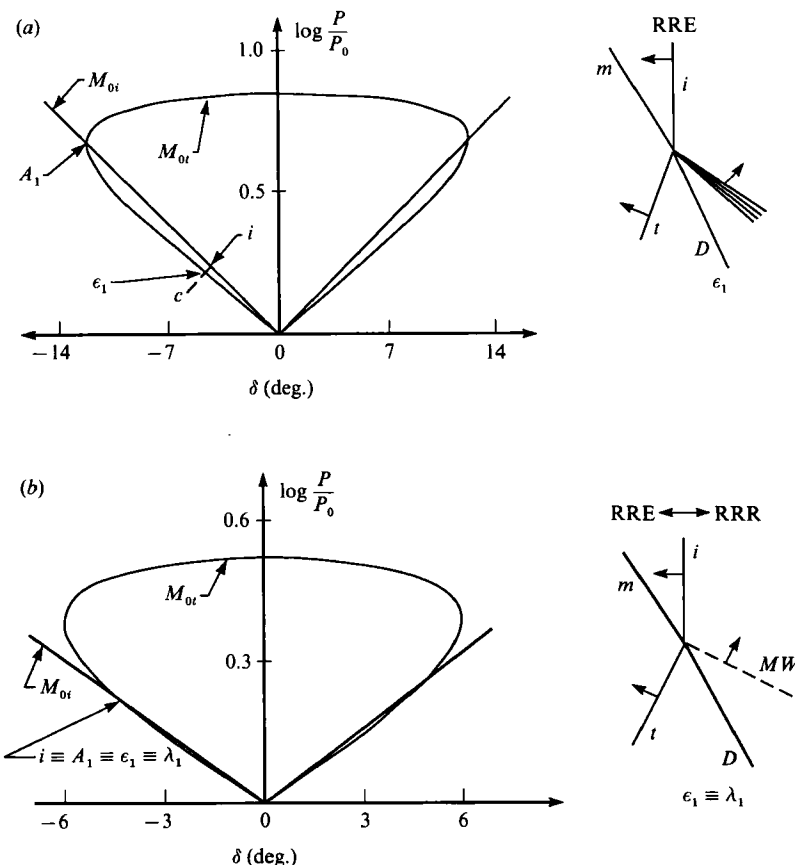


FIGURE 3(a, b). For caption see page 10.

membrane for the same refractions. In view of this we deleted it from the remainder of our computations.

*Gas contamination* The published data showed that the methane was contaminated by about 10% by volume with carbon dioxide, but that the  $\text{CO}_2$  itself was approximately pure. (Remember their volume ratio in the shock tube was about 250:1 in favour of the  $\text{CO}_2$ .) The properties of the pure and contaminated gases are presented in table 1. Contamination is a significant effect and it will be discussed below.

#### 4. Results and discussion for a weak shock refraction sequence

##### 4.1. The polar diagrams

The sequence and its polar diagrams are presented in figure 3. They are similar to the ones described by Abd-El-Fattah & Henderson although here we assume that the  $\text{CH}_4$  is not contaminated by the  $\text{CO}_2$ . When  $\alpha_i$  is comparatively small, there is a regular refraction with a reflected expansion (RRE) (figure 3a), so  $|Z_t| < |Z_i|$ ,  $R < 0$ ,  $1 > T > 0$ . Since the refraction is slow-fast,  $n < 1$ , we have by (1.11) that  $\alpha_t > \alpha_i$ , that is  $t$  is steeper than  $i$ . The reflection  $e$ , is a centred, Prandtl-Meyer, expansion fan and it is plotted in the polar diagram as the isentropic curve  $c$ . It intersects the polar for the  $t$  shock at the point  $\epsilon_1$  which defines the von Neumann solution for RRE. The

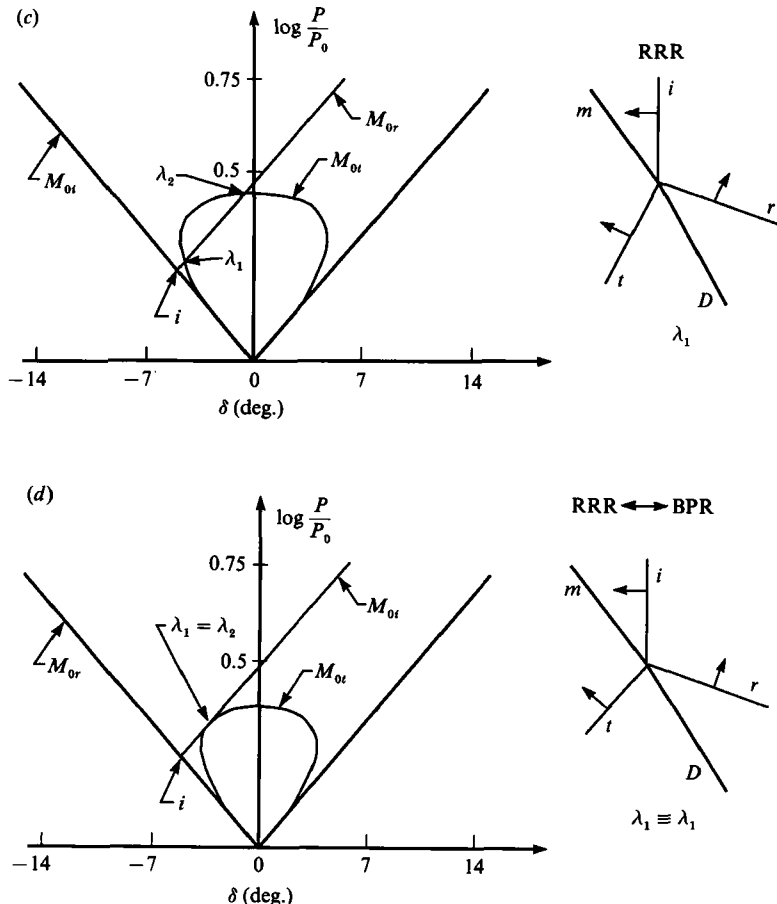


FIGURE 3(c, d). For caption see next page.

solution requires there to be continuity in the pressure and in the streamline direction  $\delta$ , everywhere along the gas interface. Although (1.2) remains valid when  $\alpha_i \neq 0$ , (1.3) must be replaced by

$$\delta_0 + \delta_1 = \delta_t, \quad (4.1)$$

where  $\delta_0$ ,  $\delta_1$  and  $\delta_t$  are the deflection angles for the  $i$ ,  $r$  and  $t$  waves respectively. This is the continuity condition for the streamline direction. It is sometimes convenient to replace (1.2) by the equivalent expression

$$(P_2 - P_1) + (P_1 - P_0) = (P_t - P_0).$$

For reflected expansions we must replace (4.1) by

$$U_{pi} \cos \beta_i + \int_1^2 \cos \beta_j dU_{pj} = U_{pt} \cos \beta_t,$$

where  $U_{pi}$ ,  $U_{pt}$ , are the driving piston velocities of the  $i$  and  $t$  shocks,  $dU_{pj}$  is the infinitesimal withdrawing piston velocity for an arbitrary  $j$ th wave in the reflected expansion, and  $\beta_i$ ,  $\beta_t$ ,  $\beta_j$  are the wave angles which are defined with respect to the disturbed gas interface (figure 2a and 2c).

If  $\alpha_i$  is now increased continuously, the polars shrink somewhat and the

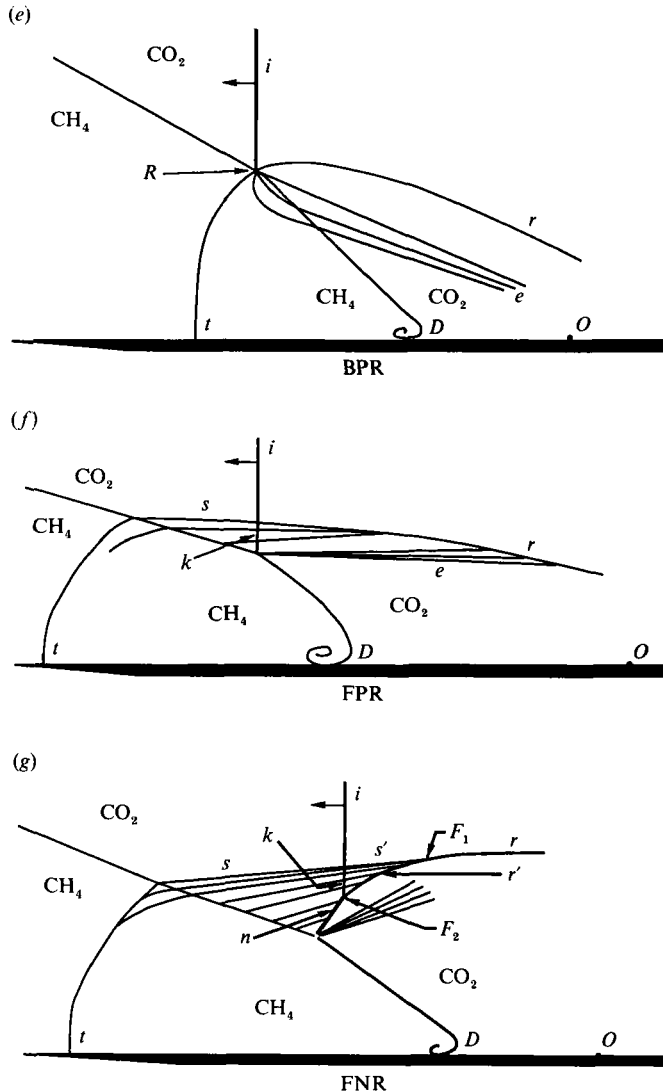


FIGURE 3. Polar diagrams for a weak shock refraction sequence with  $\xi_t = 0.78$  at a pure  $\text{CO}_2/\text{CH}_4$  gas interface. (a-c) Regular refraction, (d) transition, and (e-g) irregular refraction. (a) Reflected expansion, RRE, at  $\alpha_i = 27^\circ$ ,  $|Z_t| < |Z_i|$ ; (b) degenerate refraction at the angle of intromission  $\alpha_i = \alpha_{im} \approx 32.0592^\circ$ ,  $Z_t = Z_i$ ,  $R = 0$ ,  $T = 1$ , the condition for total energy transmission; (c) reflected shock, RRR, at  $\alpha_i = 33.27^\circ$ ,  $|Z_t| > |Z_i|$ ; (d) the shock critical angle  $\alpha_{sc} \approx 34.4885^\circ$ ; (e) bound precursor refraction, BPR,  $\alpha_t > \alpha_{sc}$ ; (f) free precursor refraction, FPR,  $s$  and  $t$  are evanescent waves; (g) free precursor von Neumann refraction, FNR,  $M_{ot}$ ,  $M_{or}$ ,  $M_{or}$ , free-stream Mach numbers upstream, and relative to the  $i$ ,  $t$ , and  $r$  shocks respectively;  $(\epsilon_1, \lambda_1, \lambda_2)$  solutions of the von Neumann regular refraction theory;  $D$ , disturbed gas interface;  $A_1$ , intersection point of the primary polars ( $i, t$ ). For other symbols see the caption to figure 2.

intersection point  $A_1$  of the primary polars ( $i, t$ ) moves downwards towards the point  $i$  which is the map of the incident shock. As this happens the strength  $|P_2 - P_1|$  of the expansion decreases and eventually vanishes at the angle of intromission  $\alpha_i = \alpha_{im} \approx 32.0592^\circ$ , which corresponds to  $\epsilon_1 \equiv i \equiv A_1$ . The reflection is reduced to a Mach line degeneracy  $|P_2 - P_1| = 0$  and the other wave impedances become equal:  $Z_t = Z_i$ ,  $R = 0$ ,  $T = 1$ . This is the condition for *total transmission*, and here also  $\alpha_t > \alpha_i$  (figures 2b

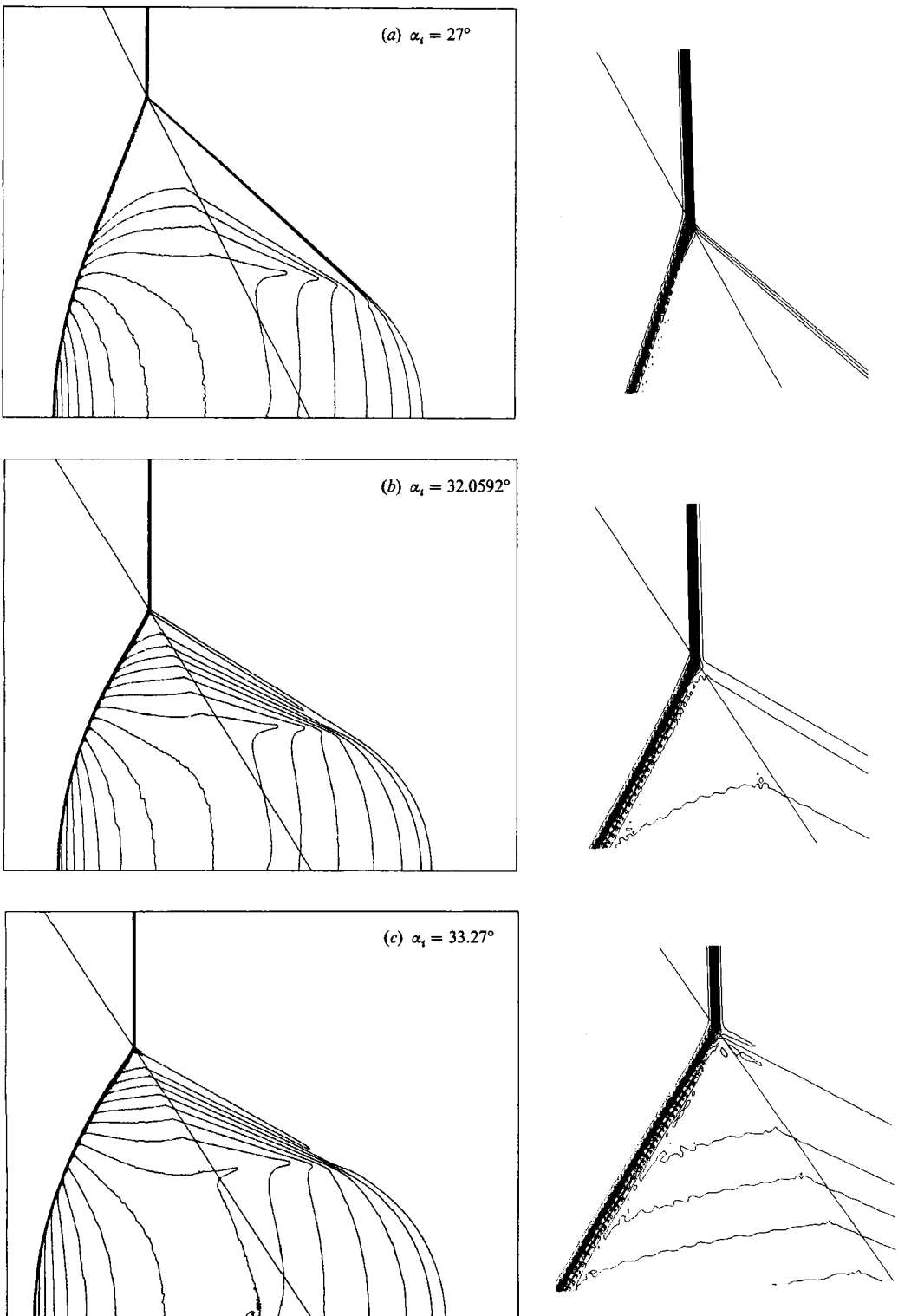


FIGURE 4(a–c). For caption see page 13.

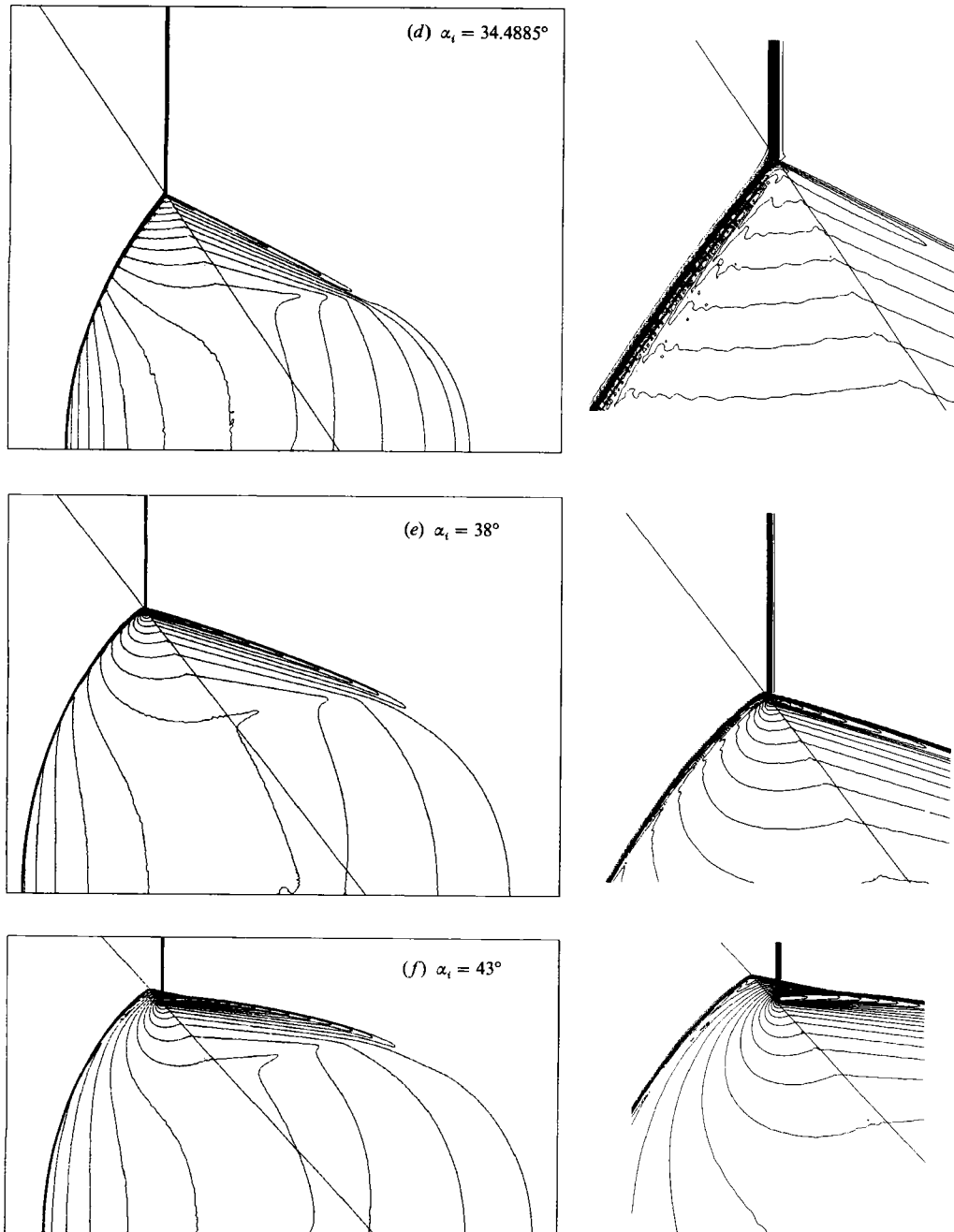


FIGURE 4(d-f). For caption see facing page.

and 3b). As  $\alpha_i$  continues to increase,  $\alpha_i > \alpha_{im}$ , the reflection becomes a shock (RRR) (figure 3c), and now  $|Z_t| > |Z_i|, R > 0, T > 1$ , with again  $\alpha_t > \alpha_i$ . The von Neumann theory gives two solutions  $\lambda_1$  and  $\lambda_2$  for RRR, but experiment shows that it is the weaker  $\lambda_1$  solution which appears physically. In this respect note that  $\lambda_1$  is the continuation of the  $\epsilon_1$  solution while  $\lambda_2$  is not; in fact at the intromission angle,  $\epsilon_1$  and  $\lambda_1$  are identical and degenerate:  $\epsilon_1 \equiv \lambda_1 \equiv A_1 \equiv i$ .

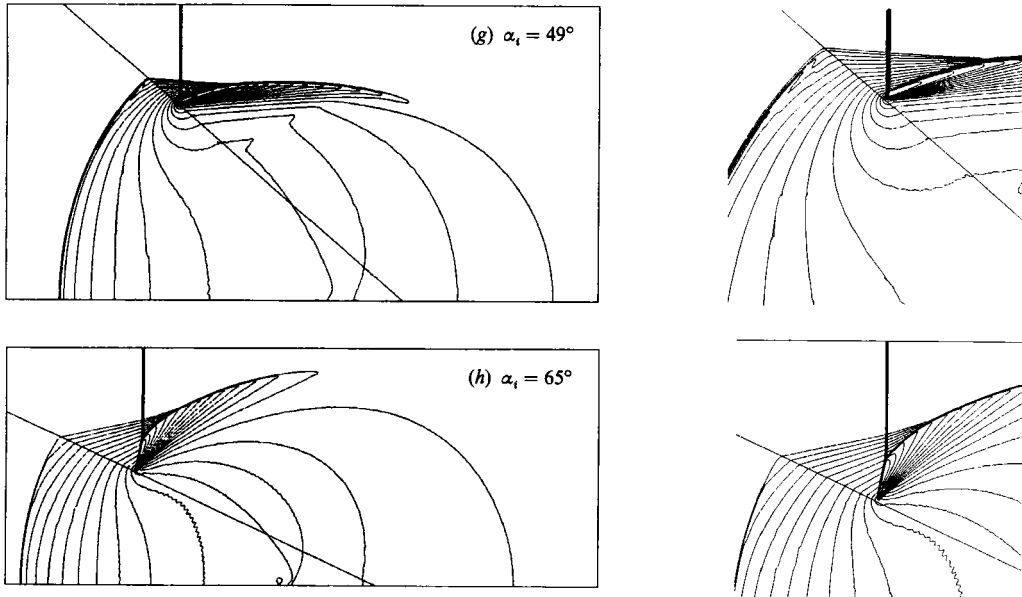


FIGURE 4. Contour plots of  $\log P$  for a weak shock refraction sequence with  $\xi_t = 0.78$  at a pure  $\text{CO}_2/\text{CH}_4$  gas interface. (a)  $\alpha_i = 27^\circ$ , RRE; (b) total transmission at the angle of intromission,  $\alpha_i = \alpha_{im} \approx 32.0592^\circ$ ; (c)  $\alpha_i = 33.27^\circ$ , RRR; (d)  $\text{RRR} \rightleftharpoons \text{BPR}$ ,  $\lambda_1 \equiv \lambda_2$ , at the shock critical angle  $\alpha_{sc} \approx 34.4885^\circ$ ; (e)  $\alpha_i = 38^\circ$ , BPR; (f)  $\alpha_i = 43^\circ$ , FPR; (g)  $\alpha_i = 49^\circ$ , FPR; (h)  $\alpha_i = 65^\circ$ , FNR. (The straight line running diagonally from upper left to lower right represents the initial, undisturbed gas interface. It is not a pressure contour.)

As  $\alpha_i$  continues to increase,  $\lambda_1$  and  $\lambda_2$  approach each other and eventually coincide,  $\lambda_1 = \lambda_2$  (figure 3d). This takes place at the *shock critical angle*  $\alpha_i = \alpha_{sc} \approx 34.488^\circ$ . In general this angle does *not* coincide with the *normal critical angle*  $\alpha_c$ , defined by (1.12), and usually occurs before it,  $\alpha_{sc} < \alpha_c$ . For  $\alpha_i > \alpha_{sc}$ , the  $\lambda_1$  and  $\lambda_2$  solutions are no longer physically significant because they are unreal. The refraction is now irregular and precursor compression waves may develop (figure 3e–g). In the experiments of both Jahn and Abd-El-Fattah & Henderson the precursors did not appear as soon as the shock critical angle was exceeded. In fact,  $\alpha_i$  had to increase somewhat beyond  $\alpha_{sc}$  before they were observed. We shall return to this point later.

#### 4.2. The numerical results for the sequence

The numerical results presented here are all for *uncontaminated* gases with *no membrane*. We believe that these results will be of more general interest than those which include the artifacts of the experiments. Selected contour plots for the sequence are shown in figure 4, a schlieren photograph from the experiments is shown in figure 5(a) and colour contour plots to compare with the schlieren photograph are shown in figure 5(b, c) (plate 1). Of course the comparison can only be qualitative because the numerical results do not include the artifacts. However, note that the numerical results exhibit all of the essential features of the flow which are found in the schlieren photo and that these features appear to be in the same relation to one another as in the schlieren. We present a more detailed comparison in §4.4 below.

Incidentally, we prefer the colour contour plots to grey scale plots of the same quantities because we believe that the eye is more sensitive to changes in colour than to changes in contrast. We find that colour reveals more detail – such as very weak

(a)

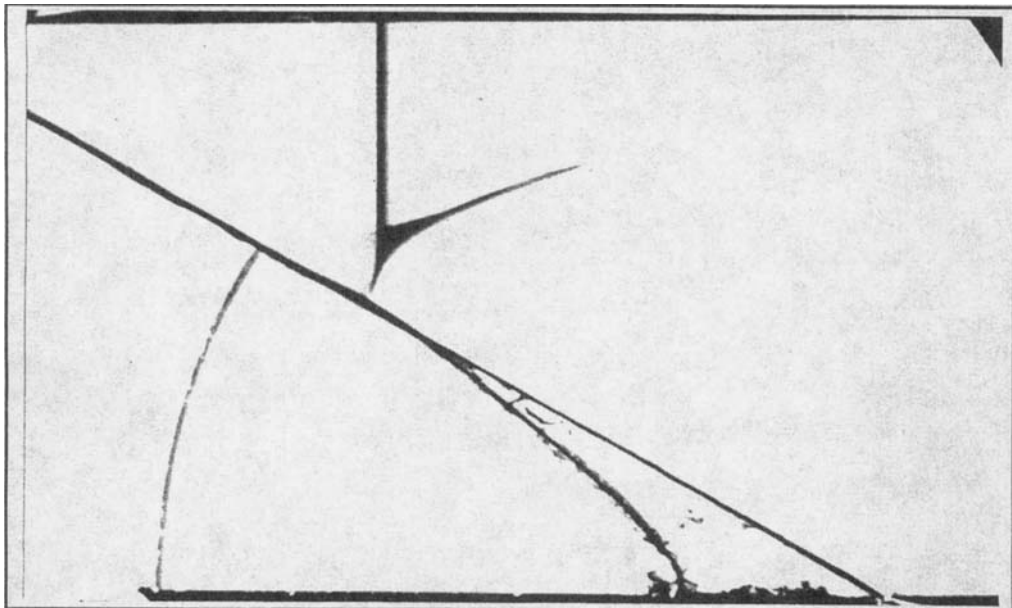


FIGURE 5. (a) Schlieren photograph and (b, c) colour contour plots for a weak irregular shock refraction, FNR at a  $\text{CO}_2/\text{CH}_4$  gas interface with  $\xi_i = 0.78$  and  $\alpha_i = 60^\circ$ .

waves or weak contact discontinuities – than black and white, or shades or grey. For example, compare the clarity of the two contact discontinuities  $cd_1$  and  $cd_2$  (figures 2*f* and 10*e*) which emanate from the two shock triple points in figures 8(*e*) and 9(*b*). Or compare the detail with which the reflected shock  $r$  and expansion  $e$  are displayed in the schlieren photograph in figure 14(*a*) versus the colour contour plots in figure 14(*b*).

#### 4.3. Structure of the weak irregular refraction systems

##### 4.3.1. The bound precursor refraction system, BPR

The regular systems RRE and RRR are well described by the von Neumann theory, and in more detail by our numerical results. When the shock critical angle is exceeded,  $\alpha_i > \alpha_{sc} \approx 34.4885^\circ$ , the RRR system becomes augmented with an expansion wave  $e$ , which appears in the receiving gas ( $\text{CH}_4$ ), and with its pressure contours apparently centred on the refraction point  $R$  (figures 3*e*, 4*e*). The contours at first diverge as they move away from  $R$ , but then swing around and refract into the incident gas ( $\text{CO}_2$ ) where they converge into a compression downstream of the reflected shock  $r$ . According to the von Neumann theory, there are no physically acceptable solutions for  $\alpha_i > \alpha_{sc}$ , and the impedances of the transmitted and reflected waves are unreal. For these reasons the system is irregular. The  $r$  and  $t$  shocks now have sharply increased curvatures near  $R$ , and furthermore  $t$  is now locally inclined forward of  $R$ ,  $\alpha_t > \frac{1}{2}\pi$  (figure 4*e*). By contrast, for the regular systems  $t$  is everywhere inclined backwards,  $\alpha_t < \frac{1}{2}\pi$  (figure 4*a-d*). Thus  $t$  is a precursor wave for  $\alpha_i > \alpha_{sc}$ , and because it apparently moves along the gas interface at the same velocity as  $i$  and  $r$ , that is (1.9) remains satisfied,  $t$  is therefore also a *bound* precursor. Like Abd-El-Fattah & Henderson we shall call this system a ‘bound precursor refraction’ (BPR). In summary a BPR differs from an RRR both by the appearance of a fourth wave

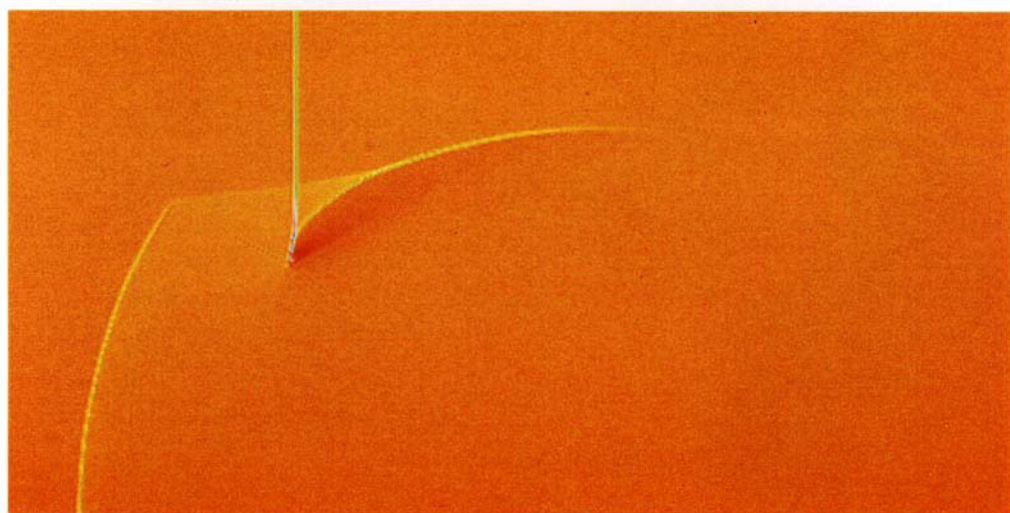
(b)



-0.328

0.231

(c)



-87.372

31.228

FIGURE 5(b,c). For caption see facing page.

(b)



(c)

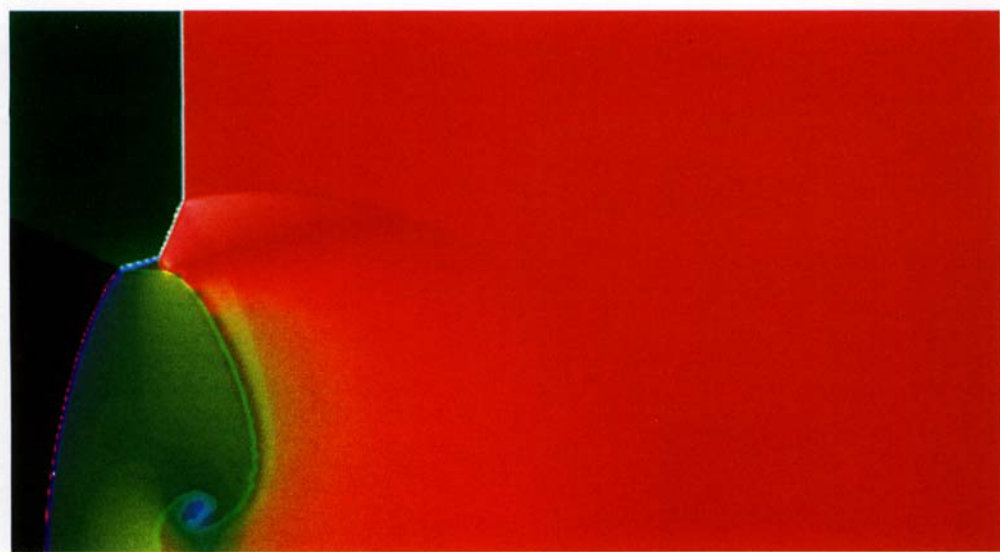


FIGURE 9(b,c). For caption see facing page.

(a)

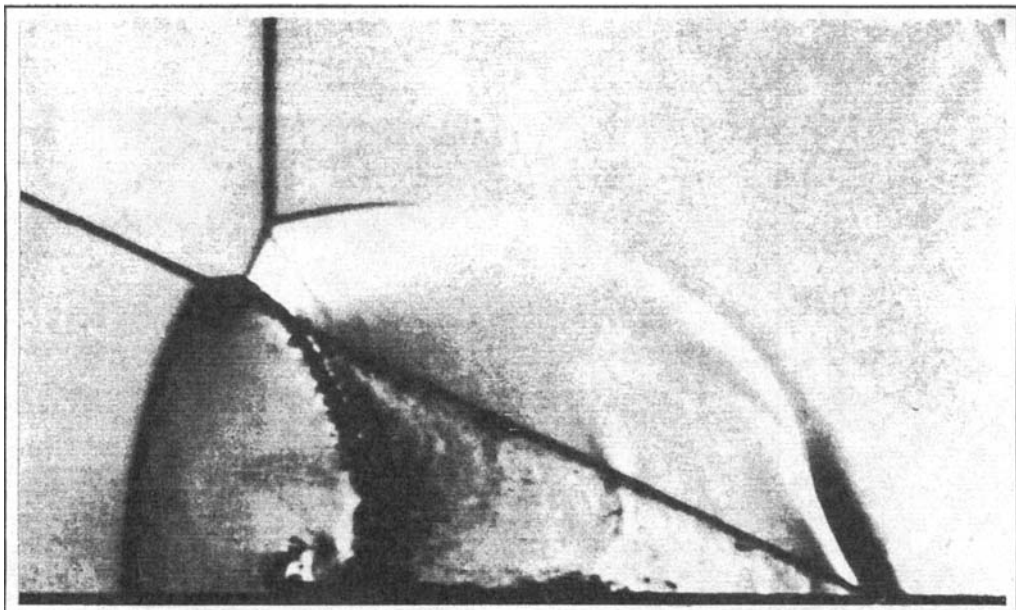


FIGURE 9. (a) Schlieren photograph and (b, c) colour contour plots for a twin Mach reflection type refraction, TMR (see figure 2f), with  $\xi_i = 0.18$  and  $\alpha_i = 66^\circ$  at a  $\text{CO}_2/\text{CH}_4$  gas interface.

and by the fact that  $t$  leans forward ( $\alpha_t > \frac{1}{2}\pi$ ) at the interface, whereas it leans backwards ( $\alpha_t < \frac{1}{2}\pi$ ) for a RRR. The detailed structure of the BPR and especially of the fourth wave as displayed in figure 4(e) have not been reported previously to our knowledge. Indeed some doubt has been expressed as to whether a BPR is a basic system or is merely an experimental artifact (Catherasoo & Sturtevant 1983). Our numerical results provide good evidence to support the existence of it as a basic system.

#### 4.3.2. The condition for the $\text{RRR} \rightleftharpoons \text{BPR}$ transition

The shock critical angle  $\alpha_{sc}$  is defined by the double root  $\lambda_1 \equiv \lambda_2$  of the von Neumann theory (figure 3d), and this amounts to a generalization of the well-known shock detachment criterion for regular/irregular transition in shock reflection. Inspection of the polar diagrams reveals that the flow downstream of the reflected shock is always supersonic,  $M_2 > 1$ , for the  $\lambda_1$  solution, and accordingly the sonic criterion (or its generalization to refraction) proposed by Hornung & Taylor (1982) cannot exist for the reflected shock. However, it can exist for the transmitted shock  $t$ , and in fact it does exist at an  $\alpha_i$  about  $1^\circ$  smaller than  $\alpha_{sc}$ . This difference is too small for experiment to discriminate, and we have not done the detailed and expensive computations necessary to decide the matter. Although the numerical data show that the  $\text{RRR} \rightleftharpoons \text{BPR}$  transition is close to the generalized detachment/sonic point for the  $t$  shock, experiment suggests that transition is delayed to values of  $\alpha_i$  somewhat larger than  $\alpha_i = \alpha_{sc}$ . In the experiments transition is somewhat obscured by the wire frame on which the membrane was mounted, and also by a thin film of silicone oil which was used to seal the wire to the shock tube windows to reduce gas leakage. In view of this we conclude that transition occurs either at the generalized detachment/sonic point, or close to it.

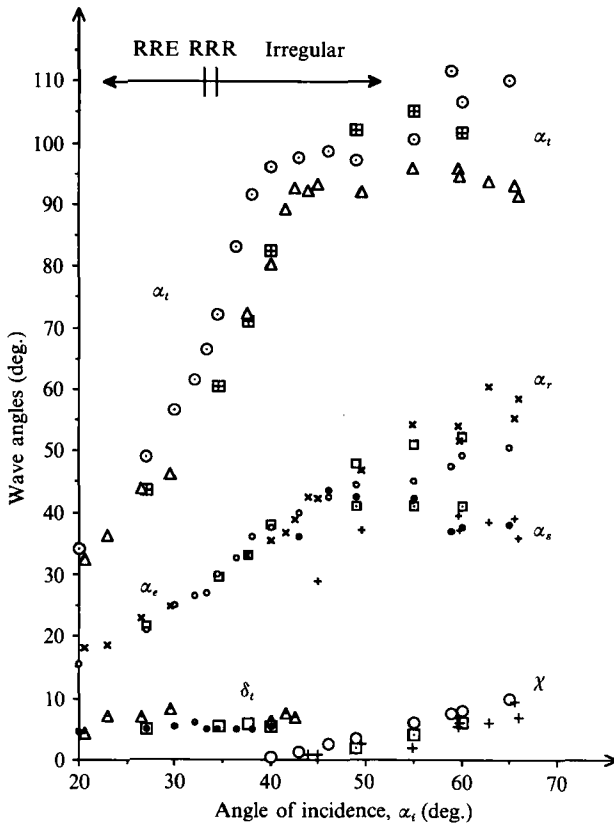


FIGURE 6. Experimental and computational wave angle data for a  $\text{CO}_2/\text{CH}_4$  gas interface with  $\xi_t = 0.78$ . Square symbols represent data from computations with a 10% contamination of the  $\text{CH}_4$  by the  $\text{CO}_2$ . Circular symbols represent data from computations with pure gases. All other symbols represent experimental data.  $\blacksquare$ ,  $\circ$ ,  $\triangle$ , transmitted shock angle  $\alpha_t$ ;  $\square$ ,  $\circ$ ,  $\times$ , reflected wave angle  $\alpha_e$  or  $\alpha_r$ ;  $\square$ ,  $\bullet$ ,  $+$ , side shock angle  $\alpha_s$ ;  $\square$ ,  $\circ$ ,  $\triangle$ , interface deflection angle  $\delta_t$ ;  $\square$ ,  $\circ$ ,  $+$ , trajectory path angle  $\chi$ ; see figure 2 for the definition of the wave angles. (Experimental data from Abd-El-Fattah & Henderson 1978b.)

It is interesting to note that the condition  $\alpha_t = \frac{1}{2}\pi$  must also be attained during the transition  $\text{RRR} \rightleftharpoons \text{BPR}$ , because as this occurs we have seen that  $(\alpha_t < \frac{1}{2}\pi) \rightarrow (\alpha_t > \frac{1}{2}\pi)$ . Therefore the condition corresponding to the normal critical angle  $\alpha_c$  defined by (1.12) is forced to occur at the same condition as the shock critical angle  $\alpha_{sc}$ , even though  $\alpha_{sc} < \alpha_c$ .

#### 4.3.3. The free precursor refraction system, FPR

With steadily increasing  $\alpha_i$ , the  $t$  wave eventually breaks loose from the  $i$  and  $r$  shocks and runs ahead of them along the gas interface (figure 4f-h). The refraction law has now been violated as with expression (1.10), and there is now a *free* precursor refraction (FPR) in which the  $t$  wave moves ever further ahead of  $i$  and  $r$  with time.

It will be noticed that the pressure contours for the  $t$  wave are now spread out at, and near, the gas interface (figure 4f-h), instead of being concentrated as for a shock (figure 4e). Thus  $t$  is a locally smeared out or *evanescent* wave. However, further away from the interface the contours do converge to form a coherent shock. The  $t$  wave is itself refracted from the  $\text{CH}_4$  back into the  $\text{CO}_2$ , which means that its refraction is

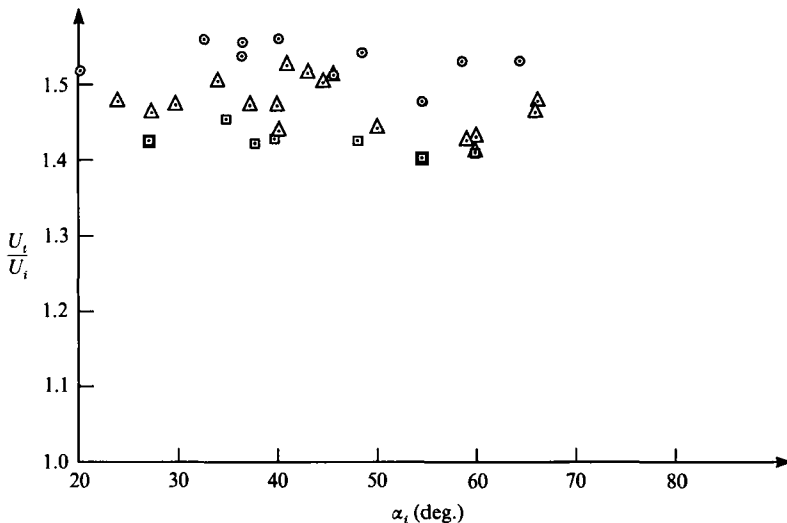


FIGURE 7. Comparison of the wave speed ratio  $U_t/U_i$  (see figure 2c) for a  $\text{CO}_2/\text{CH}_4$  gas interface with  $\xi_i = 0.78$ .  $\circ$ , Computed data for pure gases;  $\square$ , computed data for 10 % contamination of the  $\text{CH}_4$  by the  $\text{CO}_2$ ;  $\triangle$ , experimental data (from Abd-El-Fattah & Henderson 1978b).

locally fast–slow,  $n > 1$ . The wave transmitted into the  $\text{CO}_2$  is the side wave  $s$  (figure 3f, g), and it is also an evanescent wave. Since locally  $n > 1$ , then  $|\alpha_s| > |\alpha_t|$ . The contour plots show no sign of a reflected wave from the  $t$ – $s$  refraction, nor does there seem to be one in the experiments (presumably it is too weak to be resolved). Thus the local system appears to consist only of the  $t$ – $s$  pair. The  $s$  wave and the incident shock  $i$  eventually encounter, and mutually modify, each other. The  $s$  contours converge to the reflected shock  $r$  after passing through  $i$ . The modified shock  $k$ , continues to the disturbed gas interface where it is locally refracted with total internal reflection  $R = -1$ ,  $T = 0$ ,  $Z_t = 0$ . This means that  $k$  is reflected as a centred expansion wave,  $e$ . This last wave eventually overtakes  $r$  and causes almost complete mutual cancellation, so that finally a weak reflection is propagated into the downstream  $\text{CO}_2$  (figure 4f–h). It is clear from both the experimental and numerical results that  $s$  is an evanescent wave. The numerical results show that  $t$  is also evanescent but the experiments cannot resolve it. Hence the computation are predicting a new result for this wave.

It is natural to consider the conditions where a bound precursor system becomes a free precursor system or vice versa,  $\text{BPR} \rightleftharpoons \text{FPR}$ . This is associated with the spreading out of the  $t$  wave into a distributed compression near the interface and it then runs ahead of the  $i$  and  $r$  shocks along the interface. Therefore the transition occurs with the violation of the refraction law (1.9), in other words (1.10) now applies. The law is of course immediately re-established for the precursors

$$\frac{|U_s|}{\sin \alpha_s} = \frac{|U_t|}{\sin \alpha_t}.$$

#### 4.3.4. The free precursor von Neumann refraction system, FNR

Transition to yet another irregular refraction takes place as  $\alpha_t$  continues to increase. It is characterized by a weak Mach reflection appearing in the  $\text{CO}_2$ . Some pressure contours of it are presented in figure 4(h) and a schlieren photograph and colour graphics in figure 5(a–c). Abd-El-Fattah & Henderson (1978b) called this a

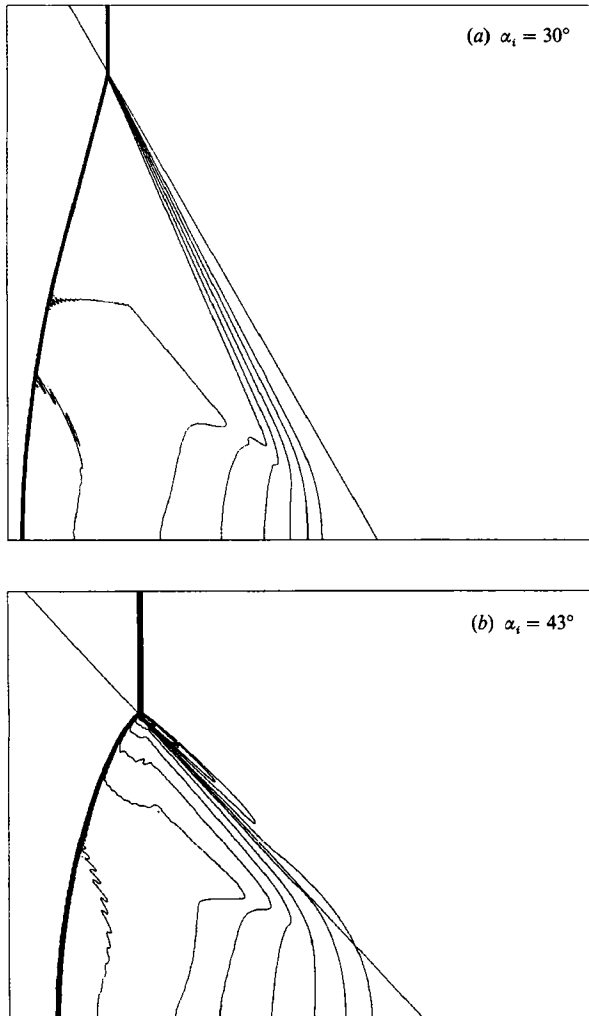


FIGURE 8(a, b). For caption see facing page.

'free precursor von Neumann refraction' (FNR). See figures 2(d), 3(g), 4(h), and 5(a-c) of this paper. The conditions for the FPR  $\rightleftharpoons$  FNR transition are not known and our computations are not sufficiently detailed to form a hypothesis with any confidence.

In summary the sequence of phenomena for the refraction of a weak shock at a slow-fast gas interface with increasing angle of incidence  $\alpha_i$  is as follows:

$$\text{RRE} \rightleftharpoons \text{RRR} \rightleftharpoons \text{BPR} \rightleftharpoons \text{FPR} \rightleftharpoons \text{FNR}.$$

This sequence seems to be generally well supported by both the computations and by the experiments.

#### 4.4. Comparison of the numerical results with experiment

In the interests of making the comparison as precise as possible we used the same values of the parameters ( $\gamma_i, \gamma_t, \mu_i, \mu_t, \xi_i, \alpha_i$ ) for our input data as Abd-El-Fattah & Henderson measured in their experiments. This included using the data for the

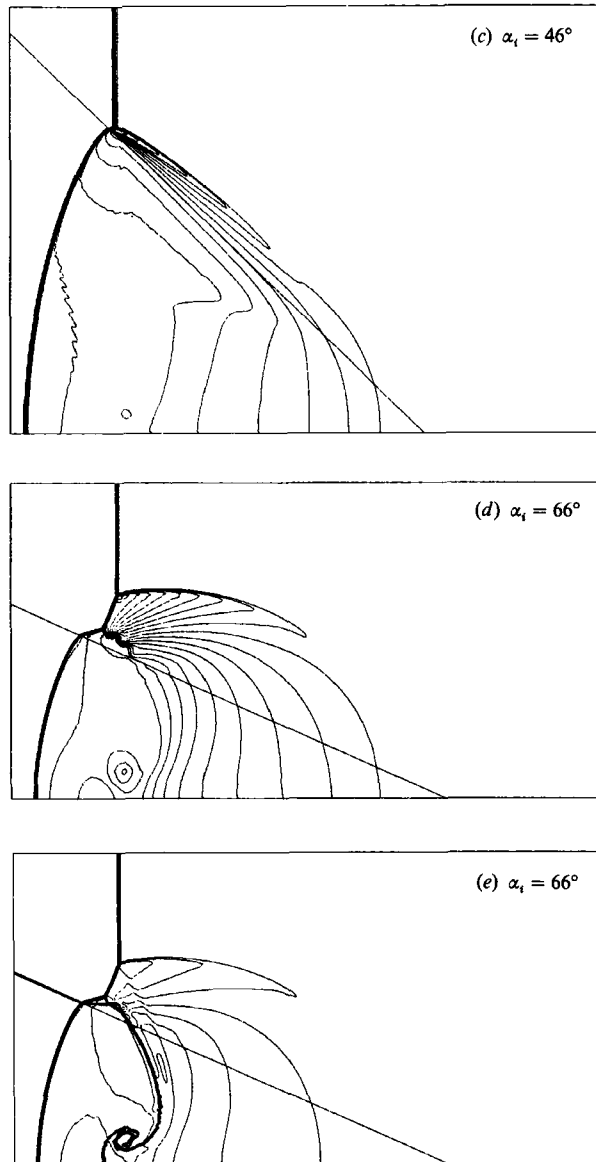


FIGURE 8. Contour plots of (a–d)  $\log P$  and (e)  $\log \rho$  from computations of a strong shock refraction sequence,  $\xi_i = 0.18$ , at a pure  $\text{CO}_2/\text{CH}_4$  gas interface. (The straight line running diagonally from upper left to lower right represents the initial, undisturbed gas interface. It is not a pressure contour.)

contaminated gas shown in table 1, and the same boundary configuration. Some of the computations were repeated for the pure gases in order to obtain an estimate of the sensitivity of the results to gas contamination. The numerical data for the pure and the contaminated gases are compared with experiment in figures 6 and 7. Figure 6 shows a variety of wave angles as well as the interface deflection angle  $\delta_t$  (figure 2a) and the trajectory path angle  $\chi$  for the intersection of the  $i, k, s$  and  $s'$  waves (figure 2d). For the regular part of the sequence,  $\text{RRE} \rightleftharpoons \text{RRR}$ , the numerical results for the

contaminated gas are everywhere in satisfactory agreement with experiment, but the corresponding results for the pure gases show a significant discrepancy for the  $\alpha_t$  data, but not for the  $\alpha_r$ ,  $\alpha_e$ , and  $\delta_t$  data. So only the  $\alpha_t$  data seem to be sensitive to contamination, and that sensitivity is greatest near transition  $\alpha_i = \alpha_{sc} \approx 34.4885^\circ$  ( $\lambda_1 \equiv \lambda_2$ ) where small variations in the contamination can cause significant changes to  $\alpha_t$ . Thus, for regular refraction the  $\alpha_t$  data are sensitive to contamination while the data for other angles are not. This is ascribed to the fact that incident and reflected waves propagate in the  $\text{CO}_2$  which is little affected by contamination because of the large fraction of the volume it occupies in the shock tube, while the  $t$  wave propagates in the  $\text{CH}_4$  and this is significantly affected (table 1).

After transition to irregular refraction the numerical data for the contaminated gas are again in agreement with experiment so long as, approximately,  $\alpha_i < 50^\circ$ ; but significant discrepancies are evident for  $\alpha_i > 50^\circ$ , particularly for the  $\alpha_t$  data. For irregular refraction the  $t$  wave is everywhere curved, and as  $\alpha_i > 50^\circ$  increased we found that this curvature became quite sharp near the gas interface. This made the choice of where to draw the tangent to  $t$  in order to measure  $\alpha_t$  at the interface increasingly uncertain. The same difficulty occurred for both the schlieren photographs and for the contour plots. We therefore looked for more robust data to compare with the experiment, which we found in the measurements of the wave velocities  $U_i$  and  $U_t$ . The numerical data for  $U_t/U_i$  are compared with experiment in figure 7. These data include the computations for the pure and the contaminated gases, and it will be noted that the results bracket the experiment data.

It should be remarked that the measurements of the gas contamination are only average values obtained after the contaminated gases had been drawn from the shock tube and individually sent to the thermal conductivity meter. Therefore the local contamination near the gas interface could have been significantly different from the average value obtained at the meter. In view of the uncertainties involved we conclude that the agreement between the numerical data and experiment is satisfactory.

## 5. Results and discussion for a strong refraction sequence

### 5.1. Wave structures in the sequence

A second series of computations was done for the  $\text{CO}_2/\text{CH}_4$  interface, except that  $i$  was now a strong shock,  $\xi_i = 0.18$ ; this work was restricted to the pure gases. Selected contours are presented in figure 8, and a schlieren photograph together with colour graphics are presented in figure 9 (plate 2). A comparison with experiment cannot be precise because the effect of gas contamination has not been taken into account in the computations. However, note that the computational results in figures 9(b) and 9(c) clearly display all of the key features of the refraction found in the schlieren photo in figure 9(a), especially the two-shock triple points  $i-n-r$  and  $s-n-r'$  and the two contact discontinuities  $cd_1$  and  $cd_2$  emanating from these triple points (figure 2f).

The polar diagrams are presented in figure 10. When  $\alpha_i$  is small enough to result in regular refraction, the von Neumann theory provides three physically acceptable solutions, namely two with reflected shocks  $\lambda_1$ ,  $\lambda_2$  and one with a reflected expansion  $\epsilon_1$  (figure 10a). It was the  $\epsilon_1$  (RRE) solution which Abd-El-Fattah & Henderson observed. With increasing  $\alpha_i$  one obtains the coincidence  $\lambda_1 \equiv \lambda_2 \equiv i \equiv A_1$ , and then the reflected shocks in the  $\lambda_1$ ,  $\lambda_2$  (RRR) solutions degenerate to Mach lines (figure 10b).

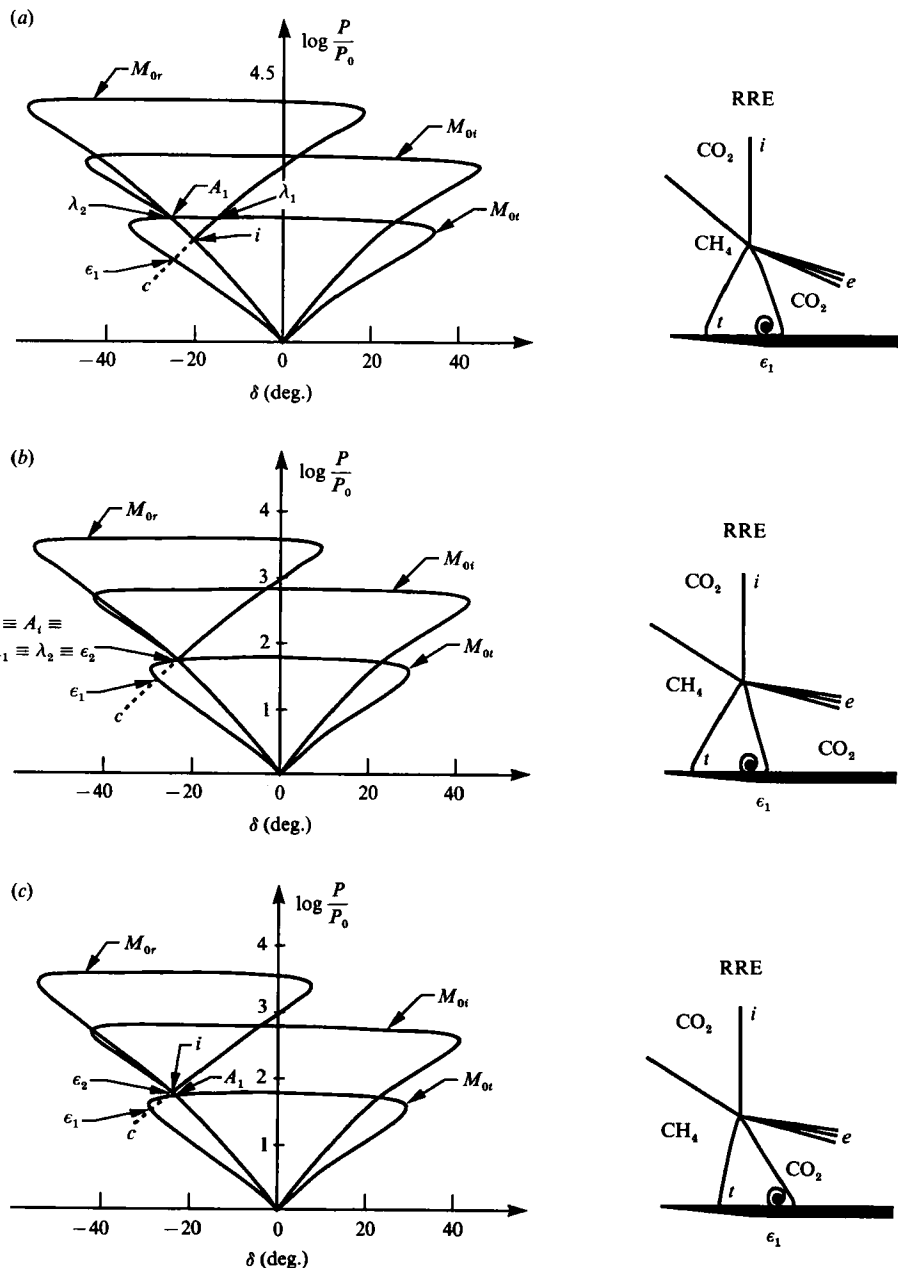


FIGURE 10(a-c). For caption see next page.

Although this takes place at the angle of intromission  $\alpha_{im} \approx 35.94^\circ$ , it has no physical significance in this case because  $\epsilon_1$  is not degenerate at this condition. Hence the impedances are *not* equal,  $Z_t \neq Z_i$ , for the solution  $\epsilon_1$  that is actually observed.

For  $\alpha_i > \alpha_{im}$ , the  $\lambda_1, \lambda_2$ , solutions are unreal and at the same time we obtain a second solution  $\epsilon_2$  of the RRE type (figure 10c). However, once more it was the  $\epsilon_1$  solution that Abd-El-Fattah & Henderson observed. Clearly, at  $\alpha_i = \alpha_{im}$  the coincidence can be extended to  $\epsilon_2$ ; thus,  $\lambda_1 \equiv \lambda_2 \equiv \epsilon_2 \equiv i \equiv A_1$ . Notice, however, that

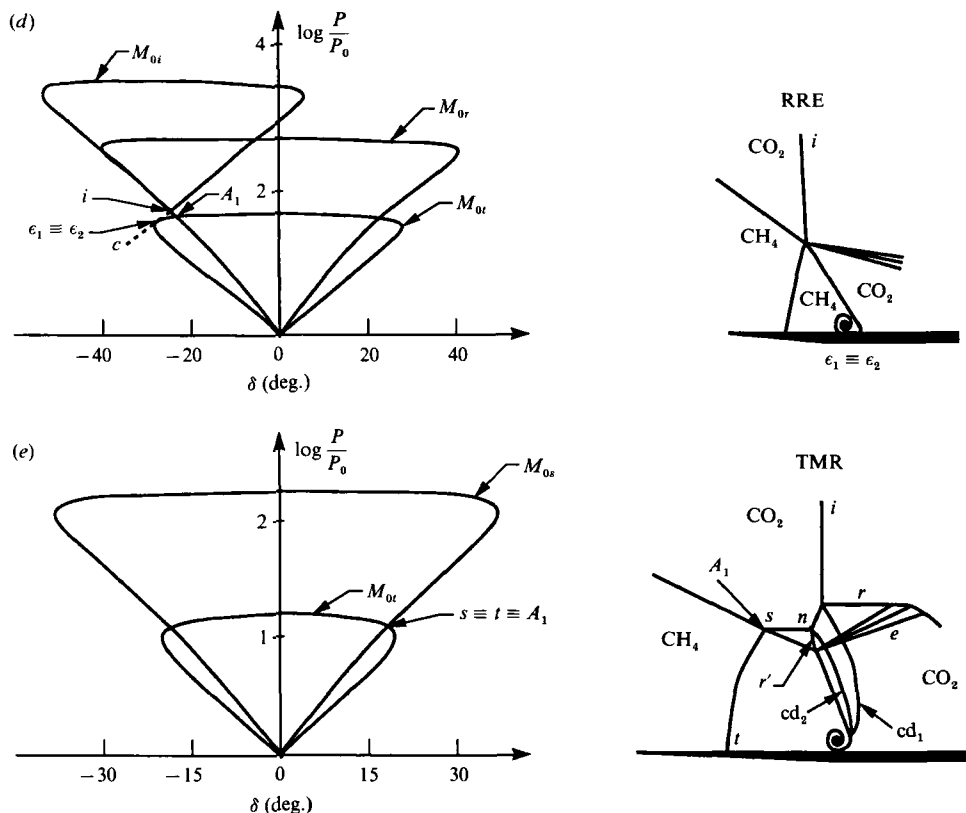


FIGURE 10. Polar diagrams for a strong shock refraction sequence with  $\xi_i = 0.18$  at a pure  $\text{CO}_2/\text{CH}_4$  gas interface. (a) RRE,  $\epsilon_1$  solution at  $\alpha_i = 30^\circ$ ; (b) RRE,  $\epsilon_1$  solution at  $\alpha_i = \alpha_{sc} = 35.95^\circ$ . Note that  $\epsilon_1$  is not a continuation of either the  $\lambda_1$ , or  $\lambda_2$  solutions, therefore the shock critical angle for  $\lambda_1 \equiv \lambda_2$  is irrelevant for transition to irregular refraction in this case; (c) RRE, at  $\alpha_i = 37^\circ$ ; note there are now two RRE solutions,  $\epsilon_1$  and  $\epsilon_2$ ; the  $\epsilon_1$  solution is observed in experiments; (d) RRE, at the relevant shock critical angle,  $\epsilon_1 \equiv \epsilon_2$ ,  $\alpha_1 = \alpha_{sc} = 46.294^\circ$ ; this is the transition condition for  $\text{RRE} \rightleftharpoons \text{TMR}$ ; (e) twin Mach reflection-refraction TMR at  $\alpha_i = 66^\circ > \alpha_{sc}$ .

the  $\epsilon_1$  solution nowhere forms a coincidence with either the  $\lambda_1, \lambda_2$  solutions as it did at the  $A_1$  point in the weak sequence. Consequently, by continuity no refraction of the RRR type can appear in this strong sequence.

As  $\alpha_i$  continues to increase one eventually obtains  $\epsilon_1 \equiv \epsilon_2$  (figure 10d), where the isentropic  $c$  is tangent to the  $t$  polar. This again occurs at the shock critical angle  $\alpha_{sc} \approx 37.79^\circ$ , but it differs from the weak series in that the coincidence is an RRE type  $\epsilon_1 \equiv \epsilon_2$ , instead of the RRR type,  $\lambda_1 \equiv \lambda_2$ .

For  $\alpha_i > \alpha_{sc}$ , the refraction is irregular and both the experiments and the computations agree that it is again a free precursor system. However, the numerical results show that both the  $t$  and the  $s$  waves are shocks and not evanescent compressions as they were in the weak sequence. Structurally the system consists of the precursor transmitted-side shock pair  $t-s$ , interacting with a single Mach reflection triplet of shocks  $i-r-n$  (figure 10e). The side shock  $s$  now interacts with the Mach shock  $n$ , modifies it and produces the second reflected shock  $r'$ . Consequently, there are two Mach reflections in the incident gas,  $i-n-r$ , and  $s-n-r'$ , the refraction will be called a 'twin Mach reflection-refraction' (TMR). The  $r'$  shock undergoes total internal reflection at the disturbed gas interface and gives rise to the reflected

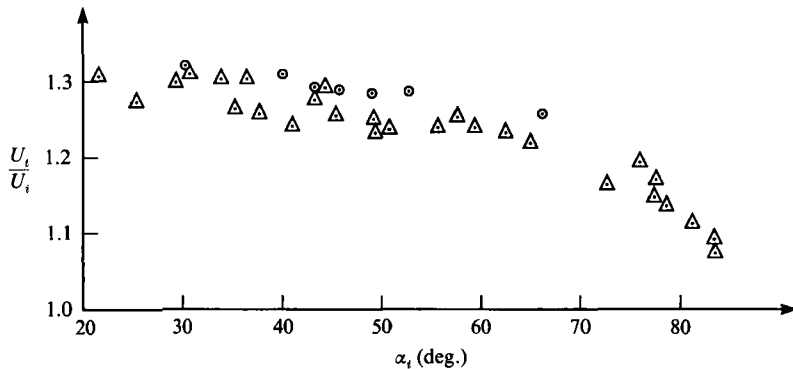


FIGURE 11. Comparison of the wave speed ratio  $U_t/U_i$  (see figure 2c) for a  $\text{CO}_2/\text{CH}_4$  gas interface with  $\xi_t = 0.18$ .  $\odot$ , Computed data for pure gases;  $\Delta$ , experimental data (from Abd-El-Fattah & Henderson 1978b).

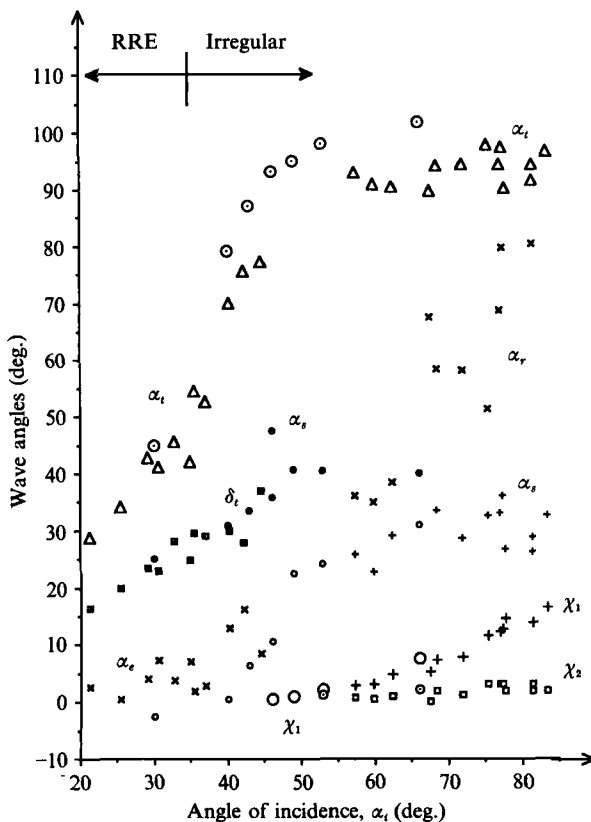


FIGURE 12. Experimental and computational wave angle data for a  $\text{CO}_2/\text{CH}_4$  refraction with  $\xi_t = 0.18$ . Circular symbols represent data from computations with pure gases. All other symbols represent experimental data.  $\odot$ ,  $\Delta$ , Transmitted shock angle  $\alpha_t$ ;  $\circ$ ,  $\times$ , reflected wave angle  $\alpha_r$  or  $\alpha_e$ ;  $\bullet$ ,  $+$ , side shock angle  $\alpha_s$ ;  $\square$ ,  $\blacksquare$ , interface deflection angle  $\delta_t$ ;  $\odot$ ,  $+$ , trajectory path angle  $\chi_1$ ;  $\odot$ ,  $\square$ , trajectory path angle  $\chi_2$ . (Experimental data from Abd-El-Fattah & Henderson 1978b.)

(a)

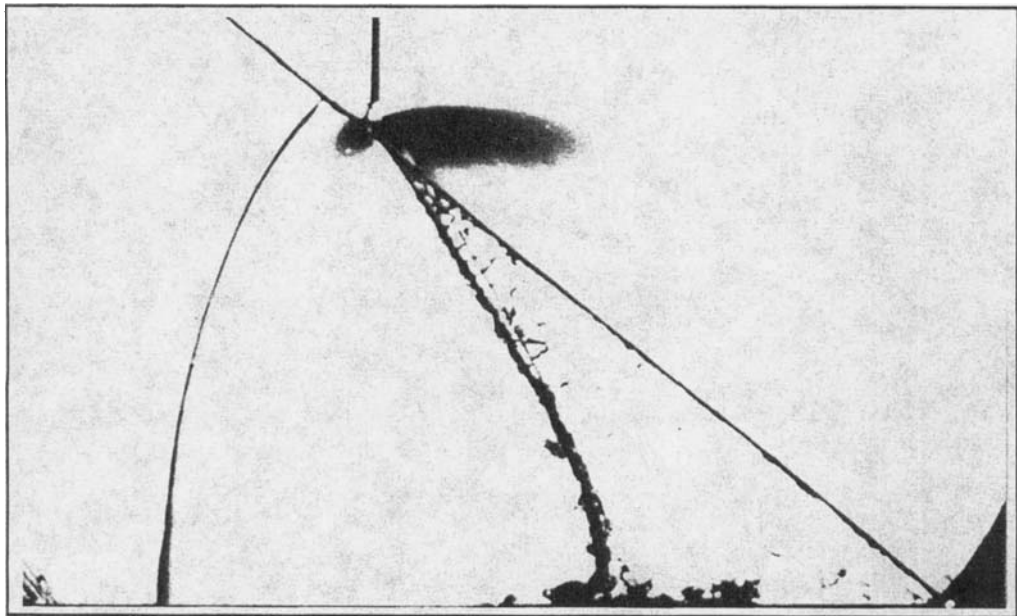


FIGURE 13. (a) Schlieren photograph and (b, c) colour contour plots for a twin regular reflection type refraction, TRR (see figure 2e)  $\xi_i = 0.53$ ,  $\alpha_i = 50.5^\circ$ , at a  $\text{CO}_2/\text{CH}_4$  gas interface. See also the caption to figure 5.

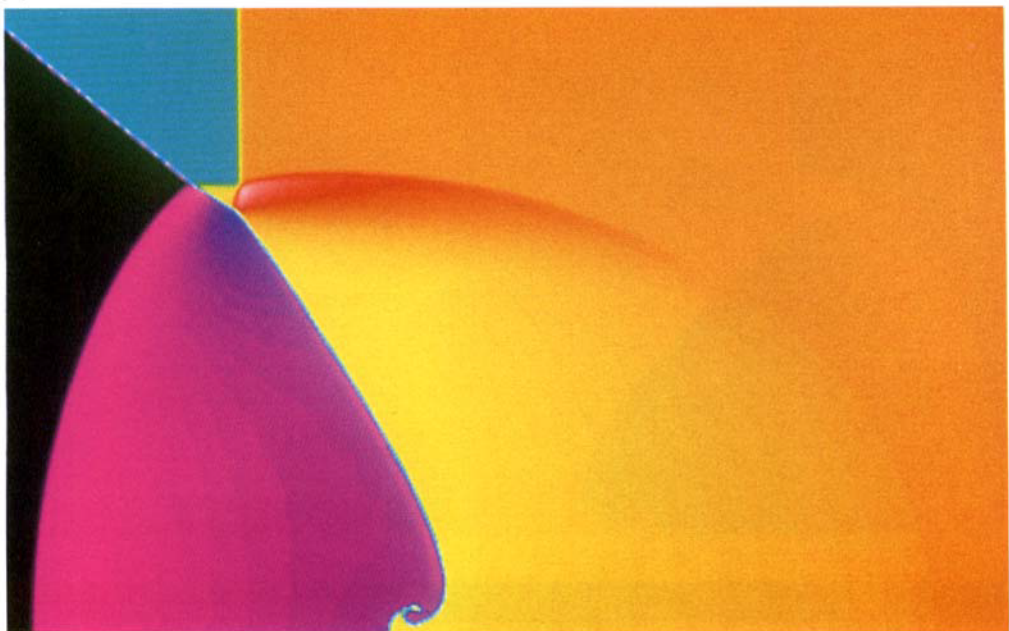
expansion  $e$ , which in turn overtakes and attenuates  $r$ . Contact discontinuities  $cd_1$  and  $cd_2$  appear at the MR triple points (figures 2f, 8e, 9a, b and 10e); of course they are not visible in figures 8(d) and 9(c) since these are contours of  $\log p$ . There are now three shear layers in the downstream flow, namely  $cd_1$  and  $cd_2$ , and the disturbed gas interface.

### 5.2. Comparison of the numerical results with experiment

The numerical results are compared with the experiments data in figures 11 and 12. As expected the discrepancy for the  $\alpha_t$  data is comparatively large because we did not take into account the gas contamination. Qualitatively it is similar to the discrepancy for the weak series in figure 6. The increasing size of the discrepancy for the irregular refraction is again attributed to the uncertainty of measuring  $\alpha_t$  with increasing curvature of the  $t$  shock near the interface. The angle data for  $\chi_1, \chi_2$ , and  $\delta_t$ , are generally in satisfactory agreement, granted the numerical and experimental uncertainties. These last measurements were made either for the  $\text{CO}_2$  flow field, or along its boundary ( $\delta_t$ ) and, as we have seen, such measurements are insensitive to gas contamination. The curvature of the reflected shock  $r$  prevented us from making reliable measurements of  $\alpha_r$ , while the short length of the side shock  $s$  similarly prevented reliable measurements of  $\alpha_s$ . The discrepancies for  $\alpha_r$  and  $\alpha_s$  are significant and are attributed to these uncertainties.

In figure 11 the numerical data for  $U_t/U_i$  display a small systematic discrepancy from the experimental data. This is qualitatively similar to the pure gas results shown in figure 7, and is ascribed to the same cause, namely gas contamination. Nevertheless, the agreement with experiment is quite reasonable.

(b)



-0.328

0.513

(c)



-28.308

138.13

FIGURE 13(b,c). For caption see facing page.

(b)



(c)



2.686

8.386

FIGURE 14(b,c). For caption see facing page.

(a)

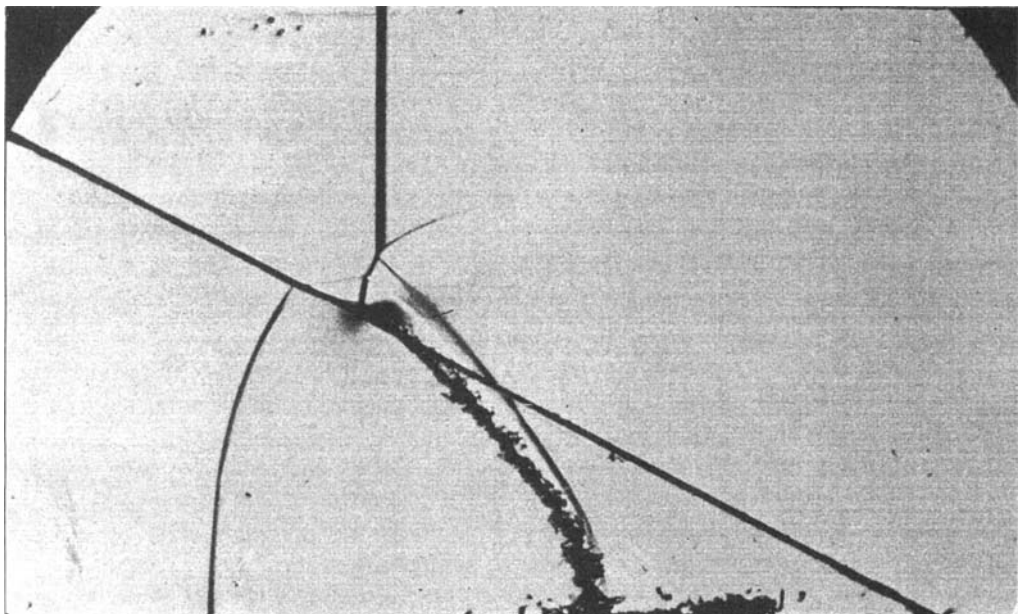


FIGURE 14. (a) Schlieren photograph and (b, c) colour contour plots for a twin von Neumann irregular refraction, TNR (Abd-El-Fattah & Henderson 1978b) at a  $\text{CO}_2/\text{CH}_4$  gas interface with  $\xi_i = 0.53$  and  $\alpha_i = 62^\circ$ .

## 6. The boundary between the strong and the weak systems

We consider how a weak irregular refraction may be changed into a strong one, or vice versa,  $\text{FNR} \rightleftharpoons \text{TMR}$ . This will be done by continuously reducing  $\xi_i$  from  $\xi_i = 0.78$  where the system is weak, to  $\xi_i = 0.18$ , where it is strong. In the following discussion the parameters  $(\gamma_i, \gamma_t, \mu_i, \mu_t)$  will be held constant and  $\alpha_i$  will be allowed to vary only slightly while  $\xi_i$  is decreased. We begin by considering the weak, irregular refraction that we call FNR at  $\xi_i = 0.78$  (figures 4*h* and 5*a–c*). As  $\xi_i$  decreases the shock triple points  $F_1, F_2$  (figures 2*f* and 3*g*) continuously approach the quadruple point  $G$  (figure 2*e*) and then for some  $\xi_i$  they coincide with it,  $F_1 \equiv F_2 \equiv G$ . The weak Mach reflection has now vanished and the number of shocks in the incident gas are reduced to four, *i–s–r–k* (figure 2*e*). If we imagine that the  $\text{CH}_4$  is replaced by a rigid medium with the same boundaries, then the four-shock interaction would amount to the twin regular reflection studied by Smith (1959). Since the *i* and *s* shocks are generally of unequal strength, their interaction is asymmetrical and a contact discontinuity arises in the downstream flow. A schlieren photograph of this refraction, obtained by Abd-El-Fattah & Henderson with  $\xi_i = 0.53$  and  $\alpha_i = 50.5^\circ$  is presented in figure 13(*a*), together with colour contour plots from the computations in figure (13*b, c*) (plate 3). We shall call it a twin regular reflection–refraction (TRR). Actually the cited authors found that this system existed for a range of  $\xi_i$  and not just for a particular value on the boundary between the strong and the weak systems. If  $\xi_i = 0.53$  is held constant and  $\alpha_i$  is now increased to  $\alpha_i = 62^\circ$ , then the four-shock system changes into the twin von Neumann system (TNR) (Abd-El-Fattah & Henderson 1978b) shown in figure 14 (plate 4). Eventually, however, as  $\xi_i$  becomes small enough the four-shock system in the TRR changes to the twin Mach reflection characteristics of a TMR at  $\xi_i = 0.18$ , and  $\alpha_i = 66^\circ$  (figures

$2f$ ,  $8d$ ,  $e$ ,  $9$ , and  $10e$ ). The condition for the TRR  $\rightleftharpoons$  TMR transition have been discussed by Smith for reflection, and Abd-El-Fattah & Henderson for refraction.

A variety of special conditions may be used to define precisely the strong/weak boundary. Some of them have been discussed by the above authors. Here we notice that for weak systems the regular/irregular transition RRR  $\rightleftharpoons$  BPR takes place at the von Neumann tangency point  $\lambda_1 \equiv \lambda_2$ , that is at  $\alpha_{sc}$ , but for strong systems the tangency condition has a different character  $\epsilon_1 \equiv \epsilon_2$ , so RRE  $\rightleftharpoons$  TMR, but again at  $\alpha_{sc}$ . It seems plausible therefore to define the strong/weak boundary at the point where *both* conditions are in coincidence,  $\lambda_1 \equiv \lambda_2 \equiv \epsilon_1 \equiv \epsilon_2 \equiv i \equiv A_1$ . For the pure gas interface  $\text{CO}_2/\text{CH}_4$  this is approximately at  $\xi_b \equiv \xi_i = 0.471$  and  $\alpha_i = 34.05^\circ$ . So an incident shock  $i$  has a weak refraction whenever  $\xi_i > \xi_b$  and a strong one when  $\xi_i < \xi_b$ .

Abd-El-Fattah & Henderson used a different condition for the boundary, based upon a generalization of the von Neumann classification for shock reflection, but the definition of the boundary is somewhat arbitrary.

There is some hint that in our results for the strong sequence  $\xi = 0.18$ , the four-shock TRR system appears immediately after transition to an irregular refraction. However, it is not resolved unequivocally, and in any event a TMR is certainly present when  $\alpha_i$  increases by only a small further amount.

Each regular or irregular wave system occurs for definite ranges of values of the system parameters  $(\gamma_i, \gamma_t, \mu_i, \mu_t, \xi_i, \alpha_i)$ , and it is possible to produce a topological plot of  $\xi_i$  versus  $\alpha_i$  for a given combination of gases  $(\gamma_i, \gamma_t, \mu_i, \mu_t)$ . Abd-El-Fattah & Henderson (1978b) did this for the  $\text{CO}_2/\text{CH}_4$  interface and we refer the interested reader there for further details.

## 7. Concluding remarks

In our computations of the weak refraction sequence we used the same input data as Abd-El-Fattah & Henderson had measured in their experiments. This included the effects of gas contamination due to leakage and diffusion across the membrane, and also the inertia of the membrane. The object was to test the validity of the computations by obtaining as precise a comparison with experiment as possible. We found that the membrane inertia made very little difference and we ignored it in our later computations. However, our data for the wave angle  $\alpha_t$  of the transmitted shock was sensitive to gas contamination, and to a lesser extent so was the wave velocity  $U_t$  data of this shock. None of the other data displayed such sensitivity, and this was ascribed to the fact that  $\alpha_t$  and  $U_t$  were measured for the  $\text{CH}_4$  component which was significantly affected by contamination (table 1) whereas the other data,  $\chi, \alpha_r, \alpha_s$ , and so on, were measured for the  $\text{CO}_2$  component which was very little affected by the contamination.

Our computations were everywhere in reasonable agreement with experiment when gas contamination was taken into account, except for the  $\alpha_t$  data when, approximately,  $\alpha_t > 50^\circ$ . That discrepancy was ascribed to the uncertainty of making accurate measurements of  $\alpha_t$  owing to the increasingly large curvature of the transmitted wave with increasing  $\alpha_t$ . This uncertainty applied to both the experimental data and to measurements made from the contour plots.

The computations were done for inviscid gases and since the results were generally in good agreement with experiment it is concluded that viscosity had no significant effect on the measurements. Presumably viscosity would be of most importance in the boundary layers at the system walls and in the region of mixing between the two

gases. The computations allowed vorticity production and transport but not viscous diffusion.

The computations resolved the structure of the bound precursor refraction (BPR), and revealed the presence of a fourth wave, which was an expansion and apparently centred on the refraction point. After transition to a free precursor system,  $BPR \rightleftharpoons FPR$ , the transmitted/side shock pair were found to be smeared out in the region of the gas interface, which we called evanescent waves.

Similar effects were found in our computations for stronger refraction and were ascribed to the same causes. Our computations displayed all the principle features found in experiment, such as local single Mach reflection-refractions, twin Mach reflection-refractions, free precursor shocks, contact discontinuities, reflected expansion waves, and so on. In particular our computations were able to accurately and sharply resolve contact discontinuities, for example those emanating from shock triple points (figures 10, 13, and 14). This has historically been a difficult task for numerical methods primarily designed to capture shocks. We conclude that the code does provide a satisfactory representation of the refraction phenomena even though it ignores the effects of viscosity and three-dimensionality.

This work was performed under the auspices of the US Department of Energy at the Lawrence Livermore National Laboratory under contract number W-7405-ENG-48 and partially supported by the Applied Mathematical Sciences subprogram of the Office of Energy Research under contract number W-7405-Eng-48 and the Defense Nuclear Agency under IACRO 88-873.

#### REFERENCES

- ABD-EL-FATTAH, A. M. & HENDERSON, L. F. 1978a *J. Fluid Mech.* **86**, 15.  
 ABD-EL-FATTAH, A. M. & HENDERSON, L. F. 1978b *J. Fluid Mech.* **89**, 79.  
 ABD-EL-FATTAH, A. M., HENDERSON, L. F. & LOZZI, A. 1976 *J. Fluid Mech.* **76**, 157.  
 BERGER, M. J. & COLELLA, P. 1989 *J. Comput. Phys.* **82**, 64.  
 BITONDO, D. 1950 *Inst. Aerophys., University of Toronto, UTIA Rep.* 7.  
 CATHERASOO, C. J. & STURTEVANT, B. 1983 *J. Fluid Mech.* **127**, 539.  
 COLELLA, P., FERGUSON, R. & GLAZ, H. M. 1990 Multifluid algorithms for Eulerian finite difference methods. Preprint in preparation.  
 COLELLA, P. & GLAZ, H. M. 1985 *J. Comput. Phys.* **59**, 264.  
 COLELLA, P. & WOODWARD, P. 1984 *J. Comput. Phys.* **54**, 174.  
 GLAZ, H. M., COLELLA, P., GLASS, I. I. & DESCHAMBAULT, R. L. 1985 *Proc. R. Soc. Lond. A* **398**, 117.  
 HAAS, J. F. & STURTEVANT, B. 1987 *J. Fluid Mech.* **181**, 41.  
 HENDERSON, L. F. 1989 *J. Fluid Mech.* **198**, 365.  
 HORNUNG, H. G. & TAYLOR, J. R. 1982 *J. Fluid Mech.* **123**, 143.  
 JAHN, R. G. 1956 *J. Fluid Mech.* **1**, 457.  
 LEER, R. G. VAN 1979 *J. Comput. Phys.* **32**, 101.  
 NEUMANN, J. VON 1943 In *Collected Works*, vol. 6, p. 1963. Pergamon.  
 NOH, W. F. & WOODWARD, P. 1976 *UCRL Preprint No. 77651*.  
 SCHWENDEMAN, D. W. 1988 *J. Fluid Mech.* **188**, 383.  
 SMITH, W. R. 1959 *Phys. Fluids* **2**, 533.  
 WHITHAM, G. B. 1958 *J. Fluid Mech.* **4**, 337.  
 WHITHAM, G. B. 1959 *J. Fluid Mech.* **5**, 369.